frontiers | Frontiers in Earth Science

TYPE Original Research
PUBLISHED 01 May 2024
DOI 10.3389/feart.2024.1343441

OPEN ACCESS

EDITED BY
Orlando Vaselli,
University of Florence, Italy

REVIEWED BY
Hui Tian,
Chinese Academy of Sciences (CAS), China
Tao Yang,
Nanjing University, China

*CORRESPONDENCE
Dan Wang,
njuwangdan@163.com

RECEIVED 23 November 2023
ACCEPTED 02 April 2024
PUBLISHED 01 May 2024

CITATION
Wang H, Sun Y, Wang D, Shu X, Cheng C and Qian P (2024), Hydrothermal activities contribute to the strong metal enrichments during early Cambrian: evidence from the comparison between black rock series in Tarim and South China.
Front. Earth Sci. 12:1343441.
doi: 10.3389/feart.2024.1343441

Hydrothermal activities contribute to the strong metal enrichments during early Cambrian: evidence from the comparison between black rock series in Tarim and South China

Hongzuo Wang[1], Yonglong Sun[2], Dan Wang[1]*, Xujie Shu[1], Cheng Cheng[1] and Peng Qian[1]

[1]School of Geographic Science, Nantong University, Nantong, China, [2]School of Geography Science, Nanjing Normal University, Nanjing, China

The early Cambrian period is a critical time in Earth's history, marked by the second oxygenation of the atmosphere (known as the Neoproterozoic Oxidation Event) and the rapid evolution of animals, as well as the worldwide large-scale deposits. Polymetallic Ni-Mo deposits have been previously reported in the black rocks at the base of the Cambrian strata on the Yangtze Block, South China, while their genesis is still controversial, and their global occurrences are uncertain. Therefore, we conduct a comprehensive analysis of trace elements and rare earth elements in the black rocks at the base of the Yurtus Formation in the Sugaitblak section (SGT) in Aksu, Tarim Block, and then make a comprehensive study by combining our and other data from the Tarim and Yangtze Block. The distribution patterns of the trace and rare earth element data from our study and another two sections in the Aksu area have shown that the black rocks in the Tarim were strongly enriched in V, Sr, Mo, Ba, and U, moderately enriched in Zn, Cu, Cr, and Pb, and slightly depleted in Ni, and Co during the early Cambrian. These enriched elements could mainly originate from the waning hydrothermal fluids, and then precipitate and preserve in sediments under anoxic environment. The comparison of trace elements in the black rocks between the Tarim and the Yangtze Block suggests that the types of enriched metal elements in these two regions were different, and metal concentrations in the Yangtze Block were much higher than those in the Tarim by 1–3 orders of magnitude. This result indicates that there are no polymetallic Ni-Mo enrichment layers in the black rocks in the Tarim during the early Cambrian, and the widespread polymetallic Ni-Mo enrichments in South China have been more likely influenced by the local hydrothermal activity. It could be further speculated that the early Cambrian period may have been an active period for seafloor hydrothermal activity, with locally different chemical components in hydrothermal fluids. Abundant metal nutrients brought by these

hydrothermal activities may have been a potential factor for the rapid evolution of life during this period.

KEYWORDS

polymetallic Ni-Mo enriched layers, rare earth elements, trace elements, black rock series, early Cambrian, Tarim

1 Introduction

The early Cambrian was a crucial period, during which almost all animal phyla on Earth suddenly appeared in a relatively short time (Shu et al., 2014; Zhang et al., 2014). This biological event is known as the famous "Cambrian Explosion" (Knoll and Carroll, 1999). Previous studies have shown that the rapid evolution of early animals are closely related to the drastic changes in the surface environment of the Earth during this period, including a dramatic increase in atmospheric and oceanic oxygen levels, as well as some significant chemical changes in the ocean (such as an increase in the concentration of elements such as N, P, Mo, U, V, etc.) (Shields-Zhou and Och, 2011; Och and Shields-Zhou, 2012; Lyons et al., 2014; Chen et al., 2015; Reinhard et al., 2017). At the same time, these chemical disturbances would lead to the formation of some economic deposits, such as widely distributed phosphate deposits, rhodochrosite deposits, and other metal deposits around the world (Cook, 1992; Jiang et al., 2007; Xu et al., 2011; Gao et al., 2021). The lower Cambrian black strata, composed of black shale and black chert, are widely distributed around the world, including the Yangtze Block in South China (Zhu et al., 2003), the Tarim Block in North China (Li et al., 2022), the Small Karatau in Kazakhstan (Litvinova, 2007), and Oman (Ramseyer et al., 2013). Previous studies have found that there are Ni-Mo sulfide deposits or Ni-Mo enrichment layers at the bottom of the lower Cambrian black shale (Niutitang Formation, Hetang Formation, and Xiaoyanxi Formation) in South China (Guo et al., 2007; Jiang et al., 2007; Lehmann et al., 2007; Gao et al., 2018). The formation of these deposits was likely closely related to fluctuations in the oceanic chemical composition and redox environment (Och and Shields-Zhou, 2012; Lan et al., 2017; Yang et al., 2022). The research on the genesis of these deposits could help with revealing the underlying causes of the biological innovation in early Cambrian.

In the past few decades, numerous studies have been conducted on the Ni-Mo enrichment layers on the Yangtze Block in South China and it has been suggested that these polymetallic enrichment layers are generally deposited in a sulfidic and anoxic marine environment (Xu et al., 2013; Han et al., 2015), but the source of these metals is still controversial. To data, there are three possible scenarios, including: 1) submarine hydrothermal origin, which means that the metal source of the Ni-Mo deposits was mainly from the metal-rich hydrothermal fluids (Steiner et al., 2001; Orberger et al., 2007; Xu et al., 2013). The deposition process requires a large amount of organic matter reducing metal ions such as Ni, Mo, and U, which were then preserved in the anoxic sediments. Therefore, the ratio of Ni, Mo, U, and other metal contents to total organic carbon (TOC) in the lower Cambrian black shale were far exceeds that of average shale; 2) seawater origin: that is, the metal source of the Ni-Mo deposits was less affected or almost unaffected by factors such as submarine hydrothermal fluids and terrestrial debris, and its high metal content mainly came from the seawater under the background of extremely low sedimentation rates during the early Cambrian (Mao et al., 2002; Lehmann et al., 2007; Lehmann et al., 2016); 3) Seawater and hydrothermal mixing origin: that is, the metal source of the Ni-Mo deposit was contributed by both submarine hydrothermal fluids and seawater at the same time (Lan et al., 2017; Yang et al., 2022).

Previous studies on Ni-Mo deposits and enrichment layers have mainly focused on the black shale deposited in early Cambrian on the Yangtze Block, and there have been relatively few studies on other Blocks. Recently, there have been some studies on the trace metal elements in the lower Cambrian black shale of the Tarim Block, and have also identified the enrichments of the metal elements (He et al., 2020; Liyuan et al., 2021; Zhu et al., 2022). However, it is unclear whether the enrichment of these metal elements exhibited the similar distribution patterns with those in South China. The comparative study on the metal enrichments in Tarim and Yangtze Blocks could help with revealing the genetic mechanisms of Ni-Mo enriched layers in early Cambrian. Therefore, we conducted the analysis of the rare earth elements and trace element contents in black shale, chert, phosphorite samples from the Yurtus Formation in the Aksu area, and combined them with other sections in the Tarim region to analyze the source of metal elements, as well as the sedimentary environments. Meanwhile, through the systematic comparison between Tarim and South China, we aim to reveal the global existence of the polymetallic Ni-Mo enrichment layers in the Lower Cambrian black shale series, and make further speculation on the genetic mechanism of polymetallic Ni-Mo enrichment layers.

2 Geological setting

The Tarim Block is one of the oldest continents in China (Zhang et al., 2012) and was once an isolated continent adjacent to northwestern Australia in the early Cambrian (Li et al., 2018). The Tarim Basin is located on the southern margin of the newly formed South Tianshan Ocean, and transformed from a rift basin to a continental margin basin against the background of the Gondwana assemblage (Zhang et al., 2009; Cawood et al., 2016). In the early Cambrian, the Tarim Basin experienced a large-scale marine transgression (Lv et al., 2020), which led to widespread deposition of a series of black rock series. These black rock series consist of a combination of black shale (containing phosphatic nodules) and chert (Figure 1A), which may be time equivalent with the lower Cambrian black strata in the Yangtze Basin of South China. The Sugaitblak section (SGT) in this study is located in the Aksu area on the northwest margin of the Tarim Basin and was deposited in the continental shelf facies (Gao and Fan, 2015; He et al., 2021; Zeng et al., 2022).

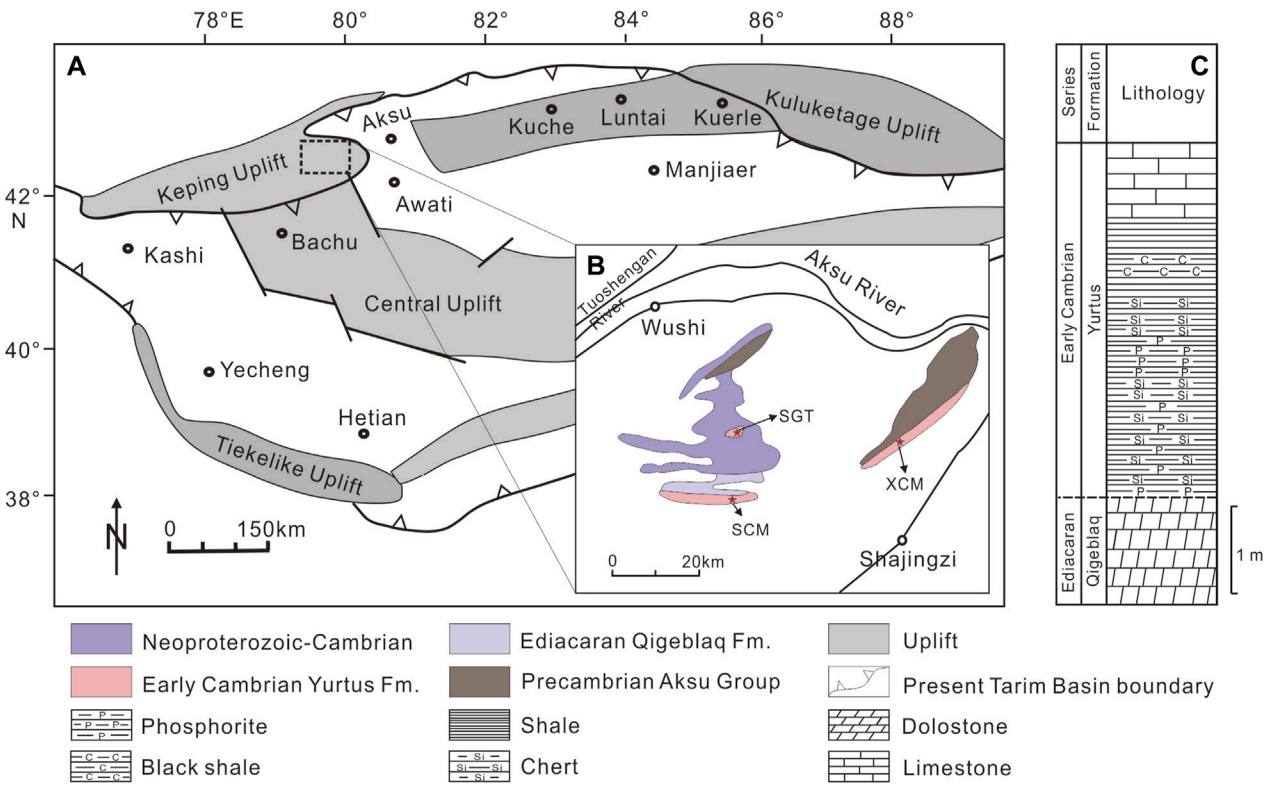

FIGURE 1
Sketch geological map of the northwestern Tarim Basin **(A)** and Aksu area **(B)**, lithological column of the Yurtus Formation **(C)** [modified after Yao et al. (2014), Wang et al. (2022)].

The Yurtus Formation of the Sugaitblak section in this study unconformably overlies the Baiyun limestone of the Qigeblaq Formation and is in conformable contact with the overlying Xiaoerblak Formation (Zhou et al., 2014; Zhou et al., 2015). The lower part of the Yurtus Formation is mainly composed of laminated black chert, black shale, and phosphorite interlayers, the middle part mainly consists of black shale, and the upper part mainly comprise limestone (Figure 1B). According to previous studies on paleontology in the Aksu area, *Asteridium-Heliosphaeridium-Comasphaeridium* (AHC) assemblages have been found in the siliceous phosphorite of the lower part of the Yurtus Formation (Xiao, 1989; Yao et al., 2005; Zhang et al., 2023). In addition, small shell fossils (SSF), such as *Anabarites trisulcatus* (Xiao, 1989; Qian et al., 2009), have also been found in the phosphoric chert of the lower part of the Yurtus Formation. Based on the fossil records of AHC and SSF, it is believed that the lower part of the Yurtus Formation belongs to the Cambrian Fortunian Stage, which is time equivalent with the phosphatic nodular black shale at the bottom of the Niutitang Formation on the Yangtze Block (Steiner et al., 2005). In addition, the presence of *Aldanella attleborensis* in the middle part of the Yurtus Formation indicates that this stratigraphic unit may belong to the Cambrian Stage 2 (Li, 2013). Previous studies have suggested that the Ni-Mo polymetallic enrichment layers in the lower part of the Nantuo/Hetang/Xiaoyanxi formations on the Yangtze Block deposited during the Cambrian Stage 2, with a Re-Os isochron age of 521 ± 5 Ma (Xu et al., 2012). Therefore, the black rock series in the lower and middle parts of the Yurtus Formation in the Tarim Basin may be time equivalent with the Ni-Mo polymetallic enrichment layers in the Yangtze region. Although some studies suggest that the *Tommotiid Lapworthella xinjiangensis* found in the upper part of the Yurtus Formation (Yue, 1992) are time equivalent with the *Sinosachites flabelliformis-Tanannuolina zhangwentangi* assemblage zone of the Meishucun Stage (Steiner et al., 2007), the widespread occurrence of *Cambroclavus fangxianensis* fossils in this stratigraphic unit (Yue and Gao, 1992) indicates the limestone in the upper part of the Yurtus Formation probably deposited in the Cambrian Stage 3 (Steiner et al., 2007). Therefore, the upper part of the Yurtus Formation is time equivalent with the upper part of the Niutitang/Hetang/Xiaoyanxi formations on the Yangtze Block.

3 Samples and methods

In this study, eight samples were sampled from the bottom of the Yurtus Formation at the Sugaitblak Section (SGT), including five black shale (SGT-5, SGT-7, -8, -9, and 10), two chert (SGT-3, SGT-6), one phosphorite sample (SGT-4), and one dolomite sample from the underlying formation (SGT-1). Fresh samples without veins were selected in the laboratory and washed with Milli-Q water, and then crushed and ground into 200 mesh and dried completely at 40°C for the further geochemical analysis. About 50 mg of sample powder (200 mesh) was weighed and digested by mixed HF and HNO_3

with a ratio of 1:3 in a Teflon-sealed digestion vessel placed in a 190°C oven for 48 h. After digestion, the sample was diluted with 3% HNO_3 for the analysis of trace and rare earth element contents. The element analysis was conducted in the laboratory of the Beijing Research Institute of Uranium Geology, using an ICP-MS. The analysis accuracy of most elements was better than 5%.

The calculation formulas for Eu anomaly and Ce anomaly are as follows (Bau, 1996; Lawrence and Kamber, 2006):

$$\delta Eu = (3 * Eu_{PAAS})/(2 * Sm_{PAAS} + Tb_{PAAS}) \quad (1)$$

$$\delta Ce = Ce_{PAAS}/(Pr_{PAAS}^{2}/Nd_{PAAS}) \quad (2)$$

The trace element data was normalized using the Paleozoic Australia Average Shale (PAAS) (Taylor and McLennan, 1985) (Figure 3). Enrichment factors are calculated to minimize the influence of debris input on the element content in the sample as much as possible.

PAAS normalized formula as follows:

$$X_{PAAS} = X_{sample}/X_{average\ shale} \quad (3)$$

Enrichment Factor (EF) formula as follows:

$$EF_{elementX} = (X_{sample}/Al_{sample})/(Al_{average\ shale}/Al_{average\ shale}) \quad (4)$$

X_{sample} represents the content of the element in the sample; $X_{average\ shale}$ represents the content of the element in PAAS (Taylor and McLennan, 1985); Al_{sample} and $Al_{average\ shale}$ represent the content of aluminum element in the sample and average shale, respectively.

4 Results

4.1 Rare earth elements

Rare Earth Element (REE) and Yttrium (Y) contents of the black rock series at the bottom of the Yurtus Formation in the Sugaitblak section (SGT) of the northwestern Tarim Basin are shown in Table 1 (data of Eu and Ce anomalies are calculated based on Eqs 1, 2), and the PAAS-normalized REE diagram is shown in Figure 2 (REE data are normalized based on Eq. 3).

The total rare earth element (ΣREE) content of the black shale is 263.94 ppm–422.2 ppm, with an average of 331.86 ppm, indicating a relatively high total REE content. The PAAS-normalized REE diagram shows 1) light REEs depletion, with a ΣLREE/ΣHREE ratio of 1.07–2.40, averaging 1.87; 2) negative Ce anomaly (δCe = 0.48–0.66); 3) slight positive Eu anomaly (δEu = 1.25–4.23); 4) slight positive Y anomalies (δY = 1.38–1.57); 5) A relatively high Y/Ho ratio of 35.5–40.5.

The rare earth element distribution pattern of the phosphorite is similar to that of the black shale, with a ΣREE of 474.43 ppm, indicating a relatively high total REE content. The PAAS-normalized REE distribution pattern shows that 1) light REEs depletion, with a ΣLREE/ΣHREE ratio of 0.90; 2) negative Ce anomaly (δCe = 0.62); 3) slight positive Eu anomaly (δEu = 1.78); 4) positive Y anomaly (δY = 1.98); 5) high Y/Ho ratio, with Y/Ho = 49.35.

The rare earth element distribution pattern of the chert sample is similar to those of black and phosphorite, but with much lower ΣREE content of 15.08–25.88 ppm and an average value of 20.48 ppm. The PAAS-normalized REE distribution pattern shows that 1) light REEs depletion, with a ΣLREE/ΣHREE ratio of 1.13–1.29; 2) negative Ce anomaly (δCe = 0.48–0.62); 3) slight positive Eu anomaly (δEu = 1.38–1.60); 4) positive Y anomaly (δY = 1.69–1.79); 5) a relatively high Y/Ho ratio, with Y/Ho= 41.34–46.33.

The rare earth element distribution pattern of the dolomite sample is similar to typical seawater, showing that 1) light REEs depletion with a ΣLREE/ΣHREE ratio of 1.32; 2) negative Ce anomaly (δCe = 0.66); 3) slight positive Eu anomaly (δEu = 1.04); 4) positive Y anomaly (δY = 1.54); 5) a relatively high Y/Ho ratio, with Y/Ho = 38.42.

4.2 Trace elements

The trace element contents are shown in Table 2. The enrichment factors of trace elements are calculated based on Eq. 4.

In the black shale, Ba, Mo, V, U, and Sr show a high degree of enrichment, among which: Ba ranges from 30635.00 to 69935.00 ppm, with an average value of 51509.40 ppm, and the enrichment factor (EF_{Ba}) ranges from 41.33 to 97.34, with an average value of 74.38; Mo ranges from 31.20 to 55.10 ppm, with an average values of 41.38 ppm, and the enrichment factor (EF_{Mo}) ranges from 25.67 to 49.05, with an average value of 38.26; V ranges from 2671.00 to 5157.00 ppm, with an average value of 3800.20 ppm, and the enrichment factor (EF_{V}) ranges from 14.65 to 40.28, with an average value of 24.25. U ranges from 45.00 to 105.00 ppm, with an average value of 66.08 ppm, and the enrichment factor (EF_{U}) ranges from 13.13 to 39.68, with an average value of 20.60; Sr ranges from 2053.00 to 3757.00 ppm, with an average value of 2918.80 ppm, and the enrichment factor (EF_{Sr}) ranges from 8.45 to 21.44, with an average value of 13.89. Meanwhile, Cr, Cu, and Pb show a moderate degree of enrichment, among which: Cr ranges from 365.00 to 764.00 ppm, with an average value of 511.60 ppm, and the enrichment factor (EF_{Cr}) ranges from 2.73 to 8.14, with an average value of 4.49; Cu ranges from 106.00 to 403.00 ppm, with an average value of 226.60 ppm. The enrichment factor of Cu (EF_{Cu}) ranges from 1.74 to 9.44, with an average value of 4.45; Pb ranges from 46.80 to 121.00 ppm, with an average value of 69.26 ppm, and the enrichment factor (EF_{Pb}) ranges from 1.93 to 7.09, with an average value of 3.39. Differently, Zn does not show significant enrichment, with a range of 75.10–201.00 ppm, an average value of 115.28 ppm, and an enrichment factor (EF_{Zn}) ranging from 0.73 to 2.07, with an average value of 1.25. On the contrary, Ni shows a moderate degree of depletion, with a range of 20.70–65.50 ppm, an average value of 35.76 ppm, and an enrichment factor (EF_{Ni}) ranging from 0.37 to 1.04, with an average value of 0.59. Co shows a significant degree of depletion, with a range of 0.90–1.88 ppm, an average value of 1.32 ppm, and an enrichment factor (EF_{Co}) ranging from 0.04 to 0.07, with an average value of 0.05.

For the phosphorite, Ba, U, Sr, and Mo show high degrees of enrichment, among which: Ba is 66027.00 ppm, with an enrichment factor (EF_{Ba}) of 891.57; U is 52.60 ppm, with an enrichment factor (EF_{U}) of 148.93; Sr is 3103.00 ppm, with an enrichment factor (EF_{Sr}) of 136.18; Mo is 21.70 ppm, with an enrichment factor (EF_{Mo}) of 190.46. Zn, V, Cu, and Ni show a moderate degree of

TABLE 1 Rare earth elements of black rock series from the Yurtus Formation in the Sugaitblak section, Aksu, Tarim Block.

Formation	Qigeblaq	Yurtus							
No.	SGT-1	SGT-3	SGT-4	SGT-5	SGT-6	SGT-7	SGT-8	SGT-9	SGT-10
Depth/m	0	0.45	0.7	0.95	1.15	1.25	1.55	1.68	1.82
Lithology	Dolostone	Chert	Phosphorite	Black shale	Chert	Black shale	Black shale	Black shale	Black shale
La	2.42	4.76	64.8	50.4	2	76.4	92.4	72.5	86.8
Ce	2.32	3.5	66.4	41.1	2.32	78.1	74.2	60.5	66.7
Pr	0.402	0.766	14	7.21	0.624	18.3	13	12.3	13.4
Nd	1.59	3.62	63	29	2.77	77.3	47.1	47.9	44.8
Sm	0.314	0.862	12.3	6.82	0.594	12.5	8.5	8.39	7.13
Eu	0.073	0.239	4.82	1.82	0.174	10.4	3.33	2.84	1.97
Gd	0.284	0.945	13.7	7.34	0.565	13.2	8.77	9.41	7.13
Tb	0.064	0.133	2.39	1.24	0.069	1.8	1.3	1.27	1.16
Dy	0.377	0.805	15.3	8.92	0.427	10.6	8.02	8.11	7.91
Y	3.65	8.71	191	89.1	4.63	102	65.8	71	72
Ho	0.095	0.188	3.87	2.29	0.112	2.7	1.8	2	1.78
Er	0.281	0.557	10.3	6.98	0.327	7.59	5.34	5.53	5.37
Tm	0.074	0.104	1.91	1.55	0.061	1.53	1.06	1.15	1.14
Yb	0.488	0.597	9.31	8.87	0.354	8.47	6.29	6.49	6.61
Lu	0.077	0.093	1.33	1.3	0.052	1.31	0.924	1.04	1.01
Y/Ho	38.42	46.33	49.35	38.91	41.34	37.78	36.56	35.5	40.45
δEu	1.04	1.38	1.78	1.25	1.59	4.23	1.95	1.69	1.35
δCe	0.66	0.62	0.62	0.66	0.48	0.52	0.6	0.55	0.48

enrichment, among which: Zn = 166.00 ppm, with an enrichment factor (EF_{Zn}) of 17.14; V = 457.00 ppm, with an average value of 307.60 ppm, and an enrichment factor (EF_{V}) of 26.00; Cu = 48.10 ppm, with an enrichment factor (EF_{Cu}) of 5.01; Ni = 10.10 ppm, with an enrichment factor (EF_{Ni}) of 1.05. Differently, Cr, Co, and Pb do not show significant enrichment. The enrichment factor (EF_{V}) of V is 26.74; Pb is 23.90 ppm, with an enrichment factor (EF_{Pb}) of 10.49; Cr is 115.00 ppm, with an enrichment factor (EF_{Cr}) of 9.18; Cu is 70.90 ppm, with an enrichment factor (EF_{Cu}) of 12.45; Ni is 36.30 ppm, with an enrichment factor (EF_{Ni}) of 5.79. However, Co shows a certain degree of depletion, with a concentration of 1.58 ppm and an enrichment factor (EF_{Co}) of 0.60.

For the chert, Mo, Sr, U, and V show high degrees of enrichment, among which Mo ranges from 4.46 to 7.45 ppm, with an average value of 5.96 ppm, and an enrichment factor (EF_{Mo}) ranging from 75.38 to 184.06, with an average value of 129.72; Sr ranges from

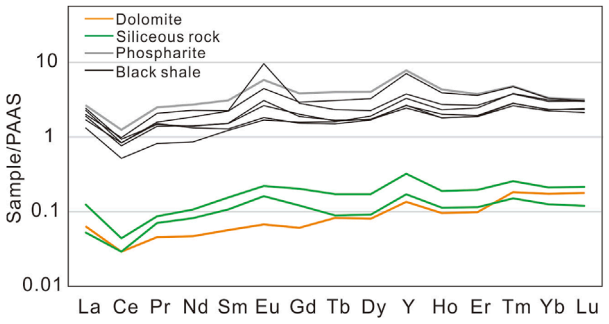

FIGURE 2
Rare earth element distribution pattern of the black rock series at the base of the Yurtus Formation in the Sugaitblak section. Data of Paleozoic Australia Average Shale (PAAS) are from Taylor and McLennan (1985).

TABLE 2 Trace elements of black rock series from the Yurtus Formation in the Sugaitblak section, Aksu, Tarim Block.

Formation	Qigeblaq	Yurtus							
No.	SGT-1	SGT-3	SGT-4	SGT-5	SGT-6	SGT-7	SGT-8	SGT-9	SGT-10
Depth/m	0	0.45	0.7	0.95	1.15	1.25	1.55	1.68	1.82
Lithology	Dolostone	Chert	Phosphorite	Black shale	Chert	Black shale	Black shale	Black shale	Black shale
Sc	1.32	6.1	2.8	18.3	4.25	20.4	17.7	17	13.8
V	19.7	265	457	5157	210	3846	2671	3531	3796
Cr	4.32	85.3	115	764	15.6	480	365	494	455
Co	3.83	1.51	1.58	0.895	0.091	1.47	1.16	1.19	1.88
Ni	78.5	7.76	36.3	20.7	2.75	26.2	24.8	41.6	65.5
Cu	3.32	55.3	70.9	403	17.5	168	106	137	319
Zn	340	44.3	166	86.3	18.2	96	75.1	118	201
Sr	52.8	1178	3103	3659	771	3757	2053	2839	2286
Zr	9.23	4.11	7.6	70	2.95	87.6	84.6	81	82.9
Mo	0.878	4.46	21.7	32.1	7.45	55.1	31.2	48.2	40.3
Ba	50.2	16348	66027	51854	14703	64332	40791	69935	30635
Th	0.594	0.27	0.756	6.29	0.192	7.05	7.71	7.49	7.61
U	2.32	4.73	52.6	105	5.76	60.9	64.2	45	55.3

771.00 to 1178.00 ppm, with an average value of 974.50 ppm, and an enrichment factor (EF_{Sr}) ranging from 95.24 to 99.55, with an average value of 97.40; U ranges from 4.73 to 5.76 ppm, with an average value of 5.25 ppm, and an enrichment factor (EF_{U}) ranging from 25.79 to 45.90, with an average value of 35.85. V ranges from 210.00 to 265.00 ppm, with an average value of 237.50 ppm, and an enrichment factor (EF_{V}) ranging from 29.86 to 34.59, with an average value of 32.22. In the meantime, Cu, Pb, Cr, and Zn show a moderate degree of enrichment: Cu ranges from 17.50 to 55.30 ppm, with an average value of 36.40 ppm, and an enrichment factor (EF_{Cu}) ranging from 8.65 to 18.69, with an average value of 13.67; Pb ranges from 10.40 to 15.10 ppm, with an average value of 12.75 ppm, and an enrichment factor (EF_{Pb}) ranging from 12.76 to 12.85, with an average value of 12.80; Cr ranges from 15.60 to 85.30 ppm, with an average value of 50.45 ppm, and an enrichment factor (EF_{Cr}) ranging from 3.50 to 13.11, with an average value of 8.31; Zn ranges from 18.20 to 44.30 ppm, with an average value of 31.25 ppm, and an enrichment factor (EF_{Zn}) ranging from 5.29 to 8.81, with an average value of 7.05. What's more, Ni shows a slight degree of enrichment, ranging from 2.75 to 7.76 ppm, with an average value of 5.26 ppm, and an enrichment factor (EF_{Ni}) ranging from 1.24 to 2.38, with an average value of 1.81. However, Co shows a slight degree of depletion, ranging from 0.09 to 1.51 ppm, with an average value of 0.80 ppm, and an enrichment factor (EF_{Co}) ranging from 0.10 to 1.11, with an average value of 0.60.

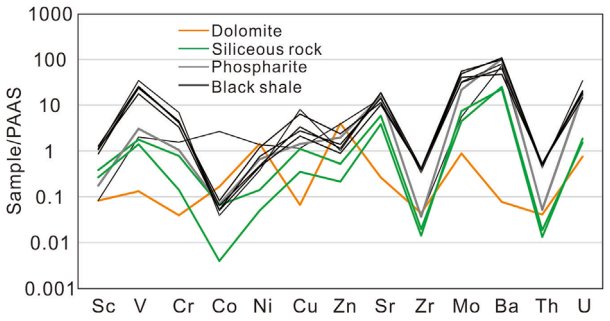

FIGURE 3
Trace elements in the black rock series at the base of the Yurtus Formation in the Sugaitblak section. Data of PAAS are from Taylor and McLennan (1985).

5 Discussion

5.1 Implication of rare earth and trace elements in the SGT section

5.1.1 Similarities and differences between different lithology

Rare earth elements in sedimentary rocks could provide good records of seawater signature (Chen et al., 2006; Ling et al., 2013;

Zhang et al., 2018). The rare earth distribution patterns of black shales (SGT-5, SGT-6, -7, -8, -9, -10), chert (SGT-3, SGT-6), and phosphorite (SGT-4) deposited in the early Cambrian are similar, though with differences in contents. This result has also been reported in other sections in the Aksu area (Yao et al., 2014).

On the other hand, the rare earth distribution patterns of the three lithology show significant differences from typical seawater (Johannesson et al., 2006) (Figure 2), and it is not yet known whether these differences originated from local or global signature, which require further analysis. Similarly, the distribution characteristics of trace elements in different lithology within the Yurtus Formation are basically the same, showing strong enrichment of V, Sr, Mo, Ba, and U; moderate enrichment of Zn, Cu, Cr, and Pb; and slight depletion of Zr, Ni, Co, Hf, and Th (Figure 3). The consistency of the rare earth and trace element distribution characteristics between the clastic rock (black shale) and chemical sedimentary rocks (phosphorites and cherts) indicates that the widespread distribution of black shales during this period can effectively record seawater information. The metal element content in black shales is barely affected by input of debris, making it an excellent object for geochemical research on the metal enrichment of early Cambrian Ocean.

5.1.2 Metal sources of the black rock series

The rare earth distribution pattern recorded in the limestone, which underlies the Yurtus Formation in this study, can effectively reflect the seawater information during the period before the deposition of the Yurtus Formation (Figure 2). The limestone sample (SGT-1) shows a "hook" shape, which is similar to the modern seawater pattern (Johannesson et al., 2006), reflecting a similar oceanic chemical environment between the late Ediacaran and modern oceans. In the Yurtus Formation, the rare earth distribution diagrams show similar patterns for black shale, cherts and phosphorites, including strong Ce negative anomalies and Eu positive anomalies (Figure 2). This phenomenon is commonly found in the lower Cambrian black rock series in the Tarim Aksu area (Yu et al., 2009; Yao et al., 2014; He et al., 2020; Li et al., 2022). Ce negative anomalies are used to trace previous redox conditions, due to the preferential absorbtion of oxidized Ce^{4+} onto particles under oxic conditions (Ling et al., 2013). The degree of Ce negative anomalies in seawater is related to the concentration of dissolved oxygen, and hence modern oxygen-rich seawater shows a strong Ce negative anomaly (Bau and Koschinsky, 2009; Tanaka et al., 2010; Ling et al., 2013). Previous studies have shown that organic matter from surface ocean biota can record information of Ce anomalies in oxidized surface seawater, which is ultimately preserved in sediments as organic matter settles (Pi et al., 2013). Therefore, the Ce negative anomalies in the samples in this study may reflect the recording of oxidized surface seawater by organic matter, which is consistent with the relatively oxidized surface environment of the Cambrian (Shields-Zhou and Och, 2011; Lyons et al., 2014). Eu is enriched in highly reducing hydrothermal fluids (Michard and Albarède, 1986; Olivarez and Owen, 1991), and Eu positive anomalies are very common in marine hydrothermal sediments (Cocherie et al., 1994). Therefore, the Eu positive anomaly in the lower Cambrian black rock series in the Tarim Aksu area could be considered as a sign of sediment influenced by seafloor hydrothermal activity (Murray et al., 1991; Douville et al., 1999; Owen et al., 1999; Yu et al., 2009; Long and Luo, 2017; He et al., 2020). In the samples of this study, the rare earth distribution pattern shows a positive Eu anomaly (1.26–4.32) and a negative Ce anomaly (0.42–0.50) (Table 1), indicating that both seawater and hydrothermal fluids were involved in the sedimentation process (Barrett et al., 1990; Mills and Elderfield, 1995). In addition, all samples in this study show similar characteristics in terms of Y/Ho ratio (Y/Ho = 35.5–40.4, average 40.5), which is much higher than the chondrite meteorite (Anders and Grevesse, 1989), and closer to the typical seawater Y/Ho ratio (Zhang et al., 1994; Nozaki et al., 1997). This indicates that the samples in this study can still reflect the seawater environment to some extent. It is preliminary inferred that the sedimentary rocks during this period were influenced by a combination of seafloor hydrothermal activity and seawater (Zhang et al., 2020). These factors can also explain the changes in the rare earth distribution pattern from the Ediacaran to the Cambrian sedimentary rocks.

As mentioned above, the distribution characteristics of trace elements in different lithologies within the Yurtus Formation are basically the same, showing strong enrichment of V, Sr, Mo, Ba, and U, while Zn, Cu, Cr, and Pb are generally enriched and Zr, Ni, Co, Hf, and Th are slightly depleted (Figure 3). Based on the enrichment of Ni, Co, and other elements in the black shale of the early Cambrian in South China (Tao et al., 2015), it is inferred that the strong enrichment of metallic elements in the sedimentary rocks may be related to basic and ultrabasic rocks, with which the hydrothermal system may be in contact, leaching out a large amount of Ni, Co, and other metallic elements. In general, basic magmas are enriched in metallic elements such as Ni and Co, while felsic magmas are enriched in metallic elements such as Zr and Hf (Sakai, 1968). In this study, neither of these two types of elements are enriched in the SGT section, suggesting that there was no contact with felsic rocks or basic and ultrabasic rocks, and that the chemical composition of the hydrothermal system is significantly different from that of South China. However, in any case, the rare earth and trace element characteristics of the samples in this study indicate that the Tarim Basin was mainly influenced by hydrothermal activity during the early Cambrian, and that the hydrothermal fluids released into the seawater partially changed the chemical composition of the seawater, ultimately recorded in the sediment and forming a pattern of mixing information from both hydrothermal and seawater.

5.2 Genetic mechanism of metal enrichments in the Tarim

Two another Cambrian sections in the Aksu area of the Tarim were compiled in this study, including the Xiaoerblak section (XCM) and the Sugaitblak No. 2 section (SCM) (Yu et al., 2009), to better explore the enrichment characteristics and genetic mechanism of metal elements in the black rock series at the base of the Cambrian strata in the Tarim (Figure 1). Previous studies have reported reliable data of rare earth and trace element contents in these two sections (Table 3; Yu et al., 2009), which have relatively complete outcrops. According to the fossil record in the Yurtus Formation (Xiao, 1989; Yao et al., 2005; Zhang et al., 2023), it can be estimated that the black rock series at the base of the Yurtus Formation in the Aksu area belongs to the Cambrian Fortunian Stage, the low-middle black

TABLE 3 Trace and rare earth elements of black rock series from the Yurtus Formation in the Xiaoerblak section (XCM) and the Sugaitblak No. 2 section (SCM) (data are from Yu et al., 2009).

No.	XCM2-1	XCM-3	XCM-5	XCM 7-1	XCM 8-1	XCM 9-1	XCM 9-2	XCM 10-1	XCM 10-2	XCM 10-3	XCM 10-4	XCM 10-5
Lithology	Black shale	Black shale	Black shale	Black shale	Black shale	Black shale	Black shale	Black shale	Black shale	Black shale	Black shale	Black shale
Sc	10	10.5	3.31	8.9	8.4	5.85	4.81	3.53	3.53	4.24	3.58	3.25
V	2039	2965	1049	12207	3976	2883	1728	1324	998	1069	290	620
Cr	1163	1057	308	1471	646	609	411	265	187	252	119	218
Co	1.58	3	2.27	2.84	9.38	2.8	5.63	7.26	6.43	4.98	2.45	1.34
Ni	38.8	46	16.7	131	303	51.8	126	111	87.5	104	47.3	55.3
Cu	217	618	53.8	1038	245	179	149	105	60.3	89.8	53.6	45.5
Zn	60.9	178	86.7	553	955	164	332	419	213	282	70.5	66
Sr	3669	374	999	1044	307	288	453	215	234	238	431	335
Zr	87.6	98.4	11	82.2	66.2	57.7	45.1	30.7	30.4	34.2	32.6	30.7
Mo	11.6	9.9	1.1	78.9	57.1	42.6	40.9	35	47.8	24	14.8	6.04
Ba	26448	3730	6335	885	652	905	901	536	378	380	484	474
Th	7.14	8.25	1.34	6.04	4.93	4.39	3.78	2.05	2.29	2.48	2.48	2.58
U	37.1	27	74.4	194.9	71.8	65.9	70.6	69.2	52	32.8	25.6	21.1
La	52.4	43.9	101	62.8	48.2	35.4	54.5	16.1	20.3	23.3	23	22.1
Ce	52	44.5	133	53.4	55.2	38.8	63.3	18.7	22.8	26.1	27.5	20.6
Pr	10.4	7.58	22.3	13	10.3	7.62	13.5	3.2	4.19	4.78	4.54	3.92
Nd	42.7	30.7	94.8	58.7	43.3	31.2	61.8	13.3	17.3	19.7	18.4	15.8
Sm	9.35	6.42	20.9	13.6	9.66	6.7	15.2	2.66	3.65	4.19	3.42	3.07
Eu	1.95	1.51	4.42	3.27	2.31	1.41	3.3	0.58	0.81	0.91	0.82	0.67
Gd	10.8	7.28	23.6	18	11.6	7.55	19.2	2.78	4.09	4.54	3.72	3.32
Tb	1.72	1.16	3.67	2.9	1.81	1.28	2.79	0.45	0.67	0.7	0.55	0.53
Y	98.7	62.8	244	216	137	96.1	174	27.8	47.7	46.6	40.4	33.7
Ho	2.43	1.56	4.96	4.84	2.91	2.24	3.69	0.66	1.03	1.04	0.79	0.74
Er	7.42	5.28	14.9	15.7	9.48	7.38	11	2.03	3.33	3.23	2.78	2.32
Tm	1.14	0.81	1.81	2.16	1.27	1.04	1.33	0.27	0.42	0.43	0.34	0.33
Yb	7.26	5.54	9.49	12.91	7.5	6.25	7.18	1.76	2.65	2.69	2.12	2.08
Lu	1.12	0.9	1.29	1.93	1.11	0.95	1.05	0.25	0.37	0.38	0.29	0.29
Dy	11	7.65	23.8	20.6	12.7	9.32	17.7	2.92	4.21	4.73	3.72	3.27
Y/Ho	40.62	40.26	49.19	44.63	47.08	42.9	47.15	42.06	46.31	44.81	50.95	45.66
δEu	0.97	1.1	1	1.05	1.1	0.96	1.01	1.05	1.03	1.05	1.18	1.04
δCe	0.59	0.69	0.73	0.54	0.65	0.6	0.62	0.7	0.65	0.65	0.71	0.61

(Continued on the following page)

TABLE 3 (*Continued*) Trace and rare earth elements of black rock series from the Yurtus Formation in the Xiaoerblak section (XCM) and the Sugaitblak No. 2 section (SCM) (data are from Yu et al., 2009).

No.	SCM1-1	SCM2-1	SCM3-1	SCM4-1	SCM4-2	SCM5-1	SCM5-2	SCM5-3	SCM5-4	SCM5-5
Lithology	Black shale	Black shale	Black shale	Black shale	Black shale	Black shale	Black shale	Black shale	Black shale	Black shale
Sc	6.83	4.6	4.07	5.76	4.75	3.55	2.78	2.36	2.59	2.27
V	1668	1338	4419	5394	2286	1537	1217	874	789	686
Cr	740	455	593	805	518	340	225	151	146	133
Co	1.53	1.76	1.7	4.08	4.06	2.81	4.3	4.56	3.8	2.93
Ni	38.3	30.9	69.2	155	118	69.1	78.7	66	63.7	60.8
Cu	278	224	364	428	241	109	84.7	65.1	50	46.6
Zn	79.5	88.1	213	503	373	165	250	211	175	159
Sr	1348	458	681	450	198	247	223	150	157	132
Zr	62	36.5	31.1	49.5	41.3	34.2	25.3	20.4	21.5	18.6
Mo	7.16	13.7	26.7	55.3	33.2	27.8	25.3	27.6	23.9	16
Ba	10059	3355	2407	2512	519	602	479	305	253	211
Th	5.13	3.2	2.46	3.66	3.11	2.72	1.94	1.45	1.59	1.36
U	21.4	33.8	89.8	148.9	65.9	45.5	46.6	40.4	28.2	20.3
La	64.05	72.2	72.7	55.5	45	41.8	35.3	23.2	21.8	18.2
Ce	68.71	88.7	83.1	54.3	51.1	47	41	26.8	24.4	20.8
Pr	13.15	14.9	14.7	11.6	10.6	8.95	8.35	4.66	4.49	3.69
Nd	59.87	62.8	68.7	51	46.5	37.2	37.5	19.1	18.5	15.3
Sm	12.91	13.6	14.2	11.6	11	8.18	8.94	3.8	3.92	3.16
Eu	2.82	2.97	2.85	2.79	2.36	1.86	1.94	0.87	0.86	0.69
Gd	15.31	15.5	15.8	14.8	13.4	9.56	10.98	4.13	4.31	3.43
Tb	2.32	2.41	2.29	2.36	2.04	1.54	1.62	0.62	0.69	0.56
Y	53.8	102	153	167	77.6	90	67.2	25.2	31.5	26
Ho	3.89	3.26	3.9	3.88	2.96	2.57	2.17	0.92	1.03	0.84
Er	11.94	10.1	11.3	12.6	9.21	8.43	6.53	3.01	3.28	2.68
Tm	1.55	1.31	1.38	1.72	1.18	1.16	0.8	0.39	0.42	0.35
Yb	9.7	7.52	9.2	10.2	6.71	6.87	4.47	2.4	2.67	2.2
Lu	1.41	1.09	1.31	1.52	1	1.03	0.65	0.33	0.38	0.31
Dy	16.93	15.7	17.2	16.7	13.5	11	10.3	4.23	4.47	3.57
Y/Ho	13.83	31.29	39.23	43.04	26.22	35.02	30.97	27.39	30.58	30.95
δEu	1.02	1.03	0.98	1.07	0.99	1.05	1.01	1.11	1.04	1.03
δCe	0.69	0.72	0.76	0.59	0.61	0.63	0.64	0.68	0.65	0.68

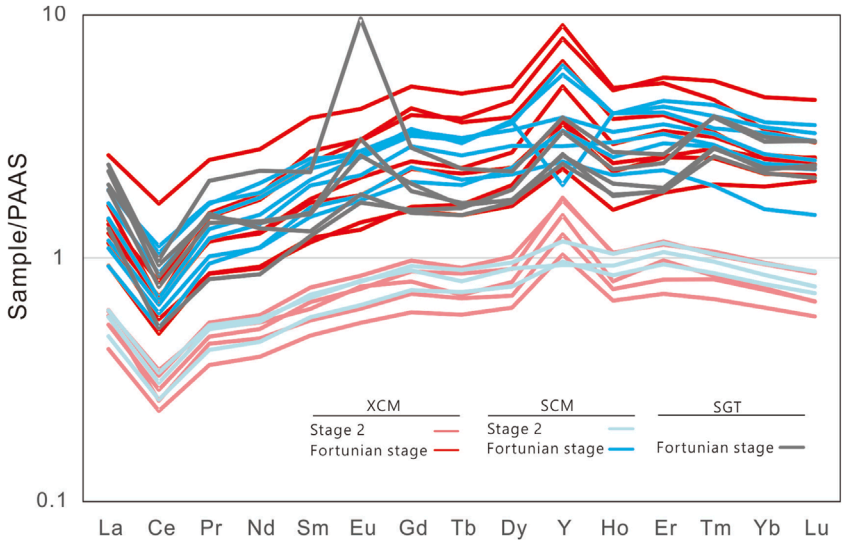

FIGURE 4
Rare earth element distribution diagram of black shale in the Yurtus Formation in the Aksu area. Data of XCM and SCM sections are from Yu et al. (2009). Data of PAAS are from Taylor and McLennan (1985).

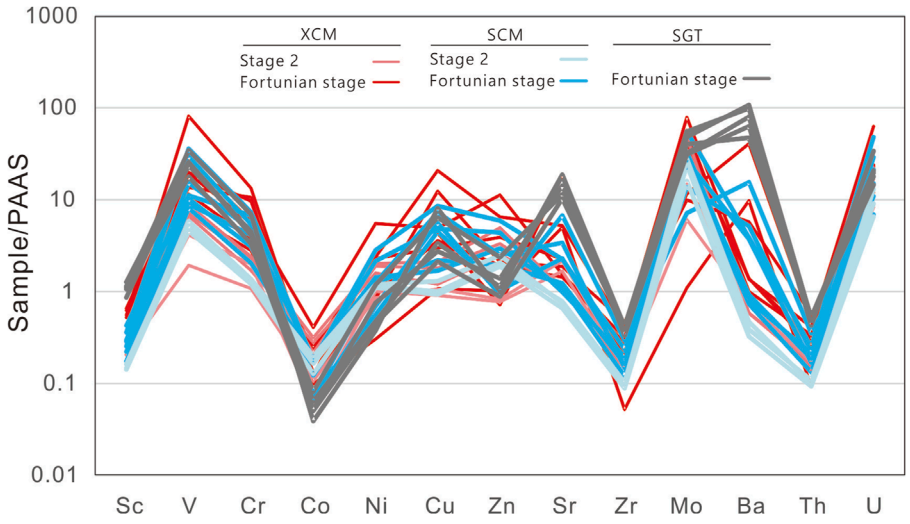

FIGURE 5
Trace element spider diagram of black shale in the Yurtus Formation in the Aksu area. Data of XCM and SCM sections are from Yu et al. (2009). Data of PAAS are from Taylor and McLennan (1985).

shale belongs to the Cambrian Stage 2, and the top limestone belongs to the Cambrian Stage 3.

On the basis of stratigraphic correlation above, rare earth and trace element data from three section have been plotted together in Figures 4, 5. Obviously, the Eu anomaly and Ba contents of the Sugaitblak section in this study are higher than those in other two sections (Figures 4, 5). The high Eu anomaly may also be the result of Ba interference during the analyzing process (Martínez-Ruiz et al., 1999; Mazumdar et al., 1999; Shields and Stille, 2001). Fortunately, there are no apparent covariance between Ba and Eu anomalies in all three sections (Figure 6), indicating the reliability of the Eu anomalies without interference of various Ba-containing compounds during the measurements. Furthermore, previous study has shown that there are barite layers at the base of the Cambrian in the Tarim region, and the abundant Ba is most likely derived from hydrothermal fluids (Zhou et al., 2015). Therefore, the spatial variations in Eu anomaly and Ba contents among the three sections should reflect that the Sugaitblak section was more strongly affected by hydrothermal activity, being closer to the hydrothermal vent, while the other two compiled sections were further away. On the other hand, it seems that the Eu anomaly is most pronounced in the Cambrian Fortunian Stage, and the rare earth element

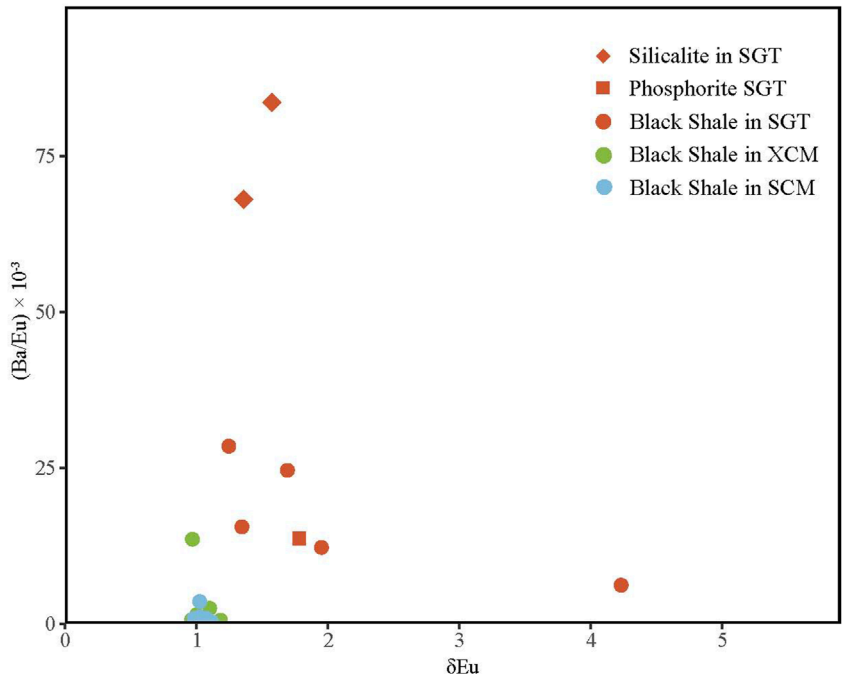

FIGURE 6
Diagram of Ba/Eu versus δEu for Sugaitblak section in this study and XCM and SCM sections in the Aksu area. Data of XCM and SCM sections are from Yu et al. (2009).

content is relatively high at this time (Figure 4). In the meantime, the trace element data also shows that the Ba content is higher in the Cambrian Fortunian Stage (Figure 5). All these results could indicate a gradual weakening trend of hydrothermal activity from the Cambrian Fortunian Stage to the Stage 2 (He et al., 2020; Zhang et al., 2020). In addition, the comprehensive rare earth distribution shows that all three sections in the Tarim region have negative Ce anomalies (Figure 4) and Y/Ho ratios close to seawater (Zhang et al., 1994; Nozaki et al., 1997) (Y/Ho = 13.83–50.95, average 39.56, with some samples having lower Y/Ho ratios, as shown in Table 1), indicating that the sediment in the early Cambrian of the Tarim Basin did indeed record information from both hydrothermal fluids and seawater, or that the elemental characteristics in the sediment were simultaneously influenced by hydrothermal fluids and seawater (Zhang et al., 2020).

Ni and Zn deposits have been suggested to be often associated with hydrothermal fissures on the seafloor, while Co deposits are often far from hydrothermal sedimentary areas. Therefore, the metal source can be determined by the relationship of these three elements in sedimentary rocks (Choi and Hariya, 1992). For the samples in the low-middle part of the Yurtus Formation in Aksu area, data from all three studied sections fell within the hydrothermal sedimentary area in Ni-Co-Zn ternary diagram (Figure 7), which is consistent with the positive Eu anomaly (Figure 4) (Yu et al., 2009). Therefore, it can be confirmed that hydrothermal fluids are an important source of metal elements for early Cambrian sediments in the Tarim. Unlike the rare earth element, the distribution pattern of the trace element for all the three studied sections (SGT, XCM, and SCM) are basically consistent (the variation trend and average value are relatively consistent, as shown in Figure 8A), without showing spatial differences. It may be due to the slow sedimentation rate of trace elements relative to rare earth elements, so that the trace element could diffuse over longer distances (Olivarez and Owen, 1991). However, trace elements show similar temporal variation pattern to rare earth elements, with the average trace element content in the Cambrian Fortunian Stage slightly higher than that in Cambrian Stage 2 (Figure 8B), indicating a gradual weakening trend of hydrothermal activity with time (He et al., 2020; Zhang et al., 2020). In addition, all three sections show depletion in Ni-Co and Zr-Hf, indicating a single hydrothermal fluid source in the study area, which brings a large amount of metal elements such as Mo, V, and U.

Redox-sensitive elements (including Mo, U, V, Co, etc.) are sensitive to the concentration of oxygen in seawater, which are usually dissolved in high-valence states under oxidizing conditions and precipitated in low-valence states under anoxic or even sulfidic conditions (Tribovillard et al., 2006). Therefore, the enrichment of redox-sensitive elements in sediment can be the good proxy to trace the marine redox conditions (Algeo and Maynard, 2008). Due to the influence of many factors on element concentrations (such as the sedimentary rates), element ratios are widely used to trace the marine redox state, including: V/(V+Ni) > 0.6, which usually indicates a reducing sedimentary environment (Hatch and Leventhal, 1992; Jones and Manning, 1994), Ni/Co < 5 represents an oxidizing sedimentary environment, 5–7 represents a suboxic sedimentary environment, and >7 indicates a sedimentary environment from suboxic to reducing (Jones and Manning, 1994). For the three studied sections in this study (SGT, XCM, SCM), V/(V+Ni) and Ni/Co ratios indicate anoxic sedimentary environment (Figure 9). On the other hand, the negative Ce anomaly in the Tarim region reflect oxygenated surface seawater recorded by

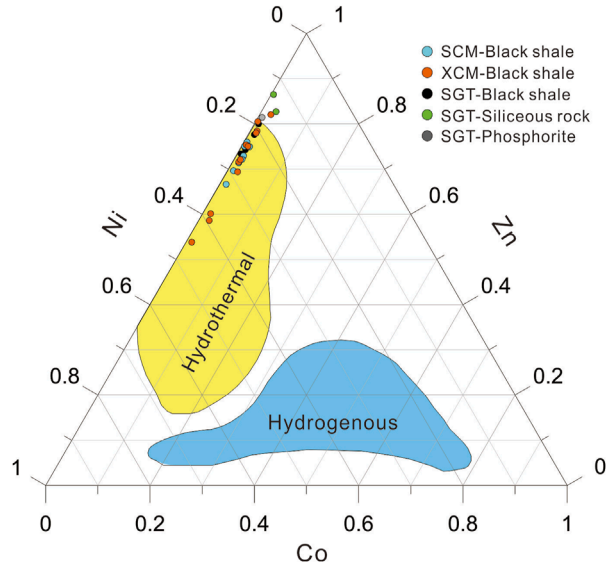

FIGURE 7
Co-Ni-Zn ternary diagram of different lithologies in the Yurtus Formation in the Aksu area [modified from Choi and Hariya (1992)]. Data of XCM and SCM sections are from Yu et al. (2009).

organic matter in the sediments (Figure 4) (Shields-Zhou and Och, 2011; Lyons et al., 2014). These results further suggest that metal elements in the early Cambrian period in the Tarim Basin probably originated from both hydrothermal fluids and seawater and were then deposited and enriched in sediment under reducing conditions in deep waters.

On the other hand, Mo and U tend to precipitate from seawater in a low-valence state under anoxic condition (Tribovillard et al., 2006). The difference is that Mo elements will rapidly precipitate in the presence of H_2S in seawater (Tribovillard et al., 2006). If Mo cannot be replenished from the open ocean in time, its content in the basin will decrease and eventually be recorded in sediments (Algeo and Rowe, 2012; Tribovillard et al., 2012). Therefore, the relationship between the enrichment factors of Mo and U in the samples (i.e., Mo-U co-variation diagram) can be used to determine the redox environment and the restrictions of the continental basin (Algeo and Tribovillard, 2009). In the Mo-U co-variation diagram, the data from three sections (SGT, XCM, SCM) in the Tarim Basin are distributed in the anoxic sedimentary environment, consistent with the implications of V/(V+Ni) and Ni/Co ratios (Figure 10). Taking together, these results indicate that the Tarim Basin was influenced by hydrothermal activity in the early Cambrian period, bringing a large amount of metal elements such as V, Mo, and U (V = 290–12,207 ppm, averaging 2334.36 ppm; Mo = 1.1–78.9 ppm, averaging 28.47 ppm, U = 20.3–194.9 ppm, averaging 58.33 ppm). These metal elements subsequently precipitated in large quantities in the reducing marine environment and were then preserved in sediments. In addition, the Mo-U co-variation diagram shows that the data points exhibit a trend where the EF_U increases faster than the EF_{Mo}, indicating that H_2S existed in the seawater of the Tarim Basin in the early Cambrian period, causing rapid sedimentation of Mo elements, and there was no timely replenishment from hydrothermal fluids and the open ocean, resulting in a relative decrease in Mo content in the seawater (Algeo and Tribovillard, 2009; Algeo and Rowe, 2012; Tribovillard et al., 2012). This suggests that the Tarim Basin was a slightly restricted basin in the early Cambrian period (Algeo et al., 2012), and further indicates that the element enrichment pattern of seawater in the Tarim Basin may at least partially record the chemical composition in the open ocean.

5.3 Global existence and genetic mechanism of metal enrichments in early Cambrian

By making a comprehensive comparison between the middle black shale of the Yurtus Formation (deposited in Cambrian Stage 2) in the Tarim Basin and the contemporaneous Ni-Mo enrichment layers in South China [data are from Table 4 (Jiang et al., 2006; Tao et al., 2015)], it has been found that the trace element enrichment on the two Blocks are significantly different (Figure 11). In South China, the Ni-Mo enriched layers are significantly enriched in Ni, V, Zn, Mo, Co, etc. (EF_{Ni} = 443.01–19994.85, average 4522.90; EF_V = 2.25–151.50, average 32.63; EF_{Zn} = 68.19–6660.13, average 1793.37; EF_{Mo} = 15897.78–3225847.88, average 481113.52). In the Tarim, except for Mo, V, and Zn elements (EF_{Mo} = 11.99–304.75, average 143.45; EF_V = 11.38–196.71, average 65.41; EF_{Zn} = 1.47–35.11, average 14.99), Cr in the black shale from the middle part of the Yurtus Formation is also enriched (EF_{Cr} = 6.37–32.32, average 18.32), while Ni only shows a slight degree of enrichment (EF_{Ni} = 1.44–16.31, average 7.82), and Co even shows a certain degree of depletion (EF_{Co} = 0.14–2.25, average 0.91). Therefore, it can be seen that the differences in trace elements in black rock series at the base of the Cambrian strata between the Tarim Basin and the South China mainly manifest in: 1) different types of enriched metal elements; 2) different degrees of element enrichment, differing by 1–3 orders of magnitude.

The Ni-Mo enriched layers/deposits at the base of the Cambrian strata in South China are important economic metal deposits (Zhang et al., 2022). Although a large amount of research has been carried out, the genesis mechanism of these deposits remains controversial. The focus of the controversy is whether metals such as Ni and Mo are only derived from seawater or whether there is a contribution from hydrothermal activity (Steiner et al., 2001; Mao et al., 2002; Lehmann et al., 2007; Orberger et al., 2007; Sláma et al., 2008; Xu et al., 2013; Lehmann et al., 2016; Lan et al., 2017; Yang et al., 2022). As is mentioned above, the Ni-Mo enriched layers in South China are mainly enriched in Mo, V, Zn, Ni and Co, while the contemporaneous black shales in Tarim are enriched in Mo, V, Zn and Cr, with Ni slight enrichment and Co depletion. It has been suggested in this and previous studies that the both South China and Tarim basin were weakly restricted basins with relatively rapid seawater renewal rates in the early Cambrian (Zhang et al., 2020; Wei et al., 2021; Wang et al., 2022). Assuming the metal enrichment in South China are solely derived from seawater, seawater was probably simultaneously enriched in Mo, V, Zn, Ni, and Co elements. Meanwhile, it has been suggested in this and previous studies that the metal enrichment in Tarim probably derived from both seawater and local hydrothermal fluids (Yao et al.,

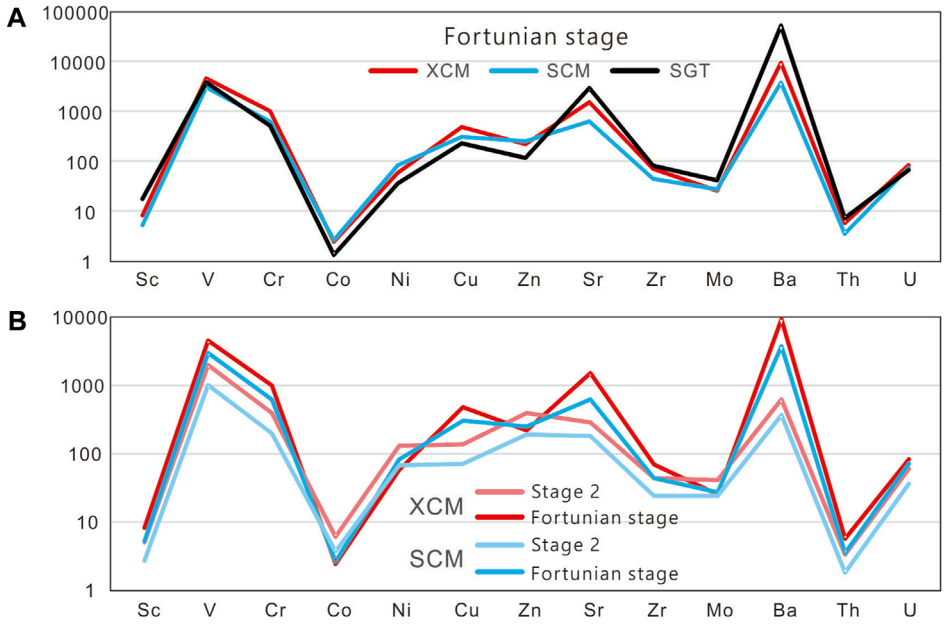

FIGURE 8
Average trace element content in the Yurtus Formation in the Aksu area. **(A)** Average trace element content in the Cambrian Fortunian Stage; **(B)** Average trace element content from Cambrian Fortunian to Stage 2. Data of XCM and SCM sections are from Yu et al. (2009).

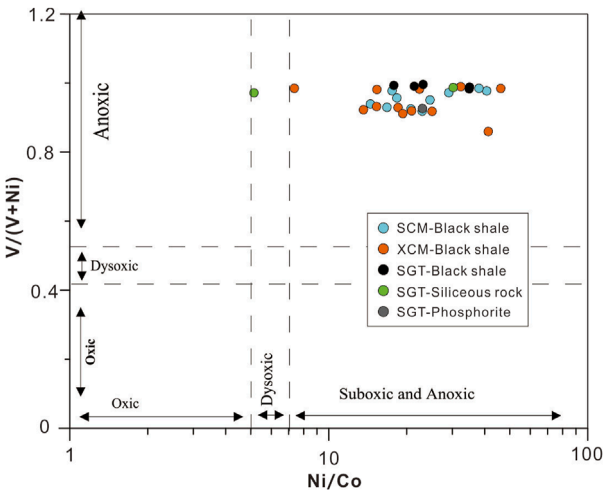

FIGURE 9
The V/(V+Ni)-Ni/Co diagram of black shale in the Yurtus Formation in the Aksu area. Data of XCM and SCM sections are from Yu et al. (2009).

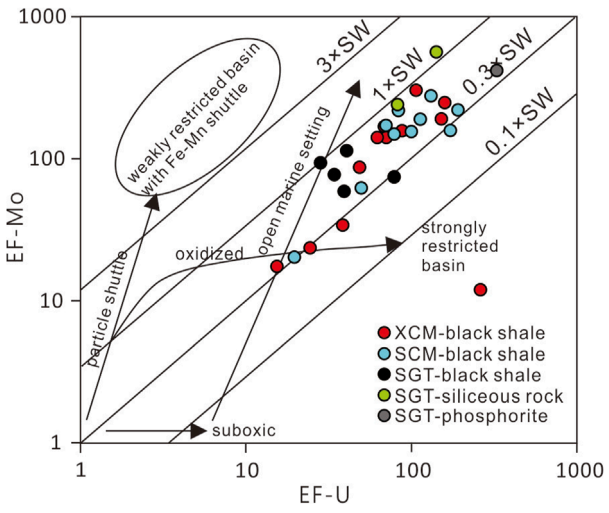

FIGURE 10
The Mo-U co-variation diagram of black shale in the Yurtus Formation in the Tarim Basin [modified according to Algeo et al. (2012), Algeo and Tribovillard (2009), Tribovillard et al. (2012)]. Data of XCM and SCM sections are from Yu et al. (2009).

2014; Zhang et al., 2020). In this case, the enrichment of Ni and Co elements should also be theoretically recorded in the Tarim Basin, unless they have been diluted by local hydrothermal fluids. In fact, Ni and Co in the contemporaneous black rock series in Tarim are much less enriched or even relatively depleted, requiring Ni and Co depletion in the hydrothermal fluid. However, the submarine hydrothermal flux into the basin was unlikely large enough to cause the dilution effect on Ni and Co elements by two or three orders of magnitude in element enrichment between the Tarim and South China. Meanwhile, the differences cannot be explained by the differences in sedimentation rates between the two basins as well. Therefore, it can basically rule out the hypothesis that the Ni-Mo enriched layers at the base of the Cambrian strata in South China are solely derived from seawater.

Indeed, many studies suggest that the Ni-Mo enriched layers at the base of the Cambrian strata in South China have involvement

TABLE 4 Trace elements of Ni-Mo enrichment layers from the Lower Cambrian Niutitang Formation, South China (data are from Han et al., 2015; Jiang et al., 2006).

Sample	Sc	V	Cr	Co	Ni	Cu	Zn	Sr	Zr	Mo	Ba	Th	U
SD6-10	1.32	217	43.5	261	20679	1997	5532	56.8	12.8	72913	211	0.33	11.2
SD3-16	6	204	38.2	316	36194	2628	95774	320	19.8	36643	161	3.4	424
SD7-1	7.81	198	56.9	437	67330	3847	62495	402	34.8	36267	267	4.46	359
SD7-2	12	237	50	300	38720	2772	66602	426	45.6	31242	288	5.77	431
SD7-3	2.83	61.5	16.6	109	14688	740	12915	298	8.91	7346	2875	1.42	156
SD8-7	5.5	105	50.5	137	18050	1116	16842	286	30.4	25647	502	3.02	219
SD8-8	2.96	71.2	25.1	150	21231	1201	10045	306	8.23	17569	259	1.75	143
SD5-4	5.96	152	51.3	275	48284	2530	115515	322	22.3	37492	1041	3.72	512
SD1-6	7.08	552	79.9	397	51009	2545	14637	278	70.1	40082	403	4.32	373
JL-1	5.13	151	48.8	409	70292	3314	116712	294	17.4	29857	2173	3.01	520
DJLZ2-1	2.5	158	51.7	368	30347	3339	26175	74.1	18	84922	1802	1.24	74.3
DJLZ3-1	7.04	163	38.5	180	19942	1484	35800	414	35.5	30714	481	3.34	257
DJLZ3-2	8.42	184	50.5	313	41538	2440	49439	312	31.5	49905	634	3.72	354
HN-1a	0.97	52.8	22.9	9.62	9237	814	1284	46.2	1.06	2027	27	1.13	57.2
HN-1b	0.1	14.9	6.73	0.45	615	68.7	204	3.87	0.99	552	66.6	0.17	16.6
HN-1c	0.3	358	39.7	42.6	7381	248	390	7.44	4.98	26973	40.3	0.23	90.6
HN-1d	0.35	149	17.6	3.52	595	24	39.7	2.17	11	1407	128	0.1	5.72
HN-2a	0.87	25.4	13.1	8.49	8789	429	1739	142	0.4	1203	40	0.97	61.9
HN-2b	0.18	10.4	6.5	0.57	751	74.9	194	22.2	0.43	490	25	0.45	34.2
HN-2c	0.3	152	23.2	41.8	9792	451	374	4.04	4.71	19677	8.64	0.13	123
HN-2d	0.46	102	16.8	3.66	688	40.4	39.7	2.1	11.1	1007	119	0.08	6.8
GZ-1a	1.49	64.4	1.6	2.72	578	62.4	162	324	2.06	369	134	1.52	28.5
GZ-1b	0.09	7.65	0.3	0.88	53.5	6.79	101	17.6	1	76.8	157	0.3	17.3
GZ-1c	0.61	283	14.7	9.8	1494	199	235	17.9	6.27	418	354	0.46	20.5
GZ-1d	0.4	97	6.11	0.41	64.1	9.02	18.6	7.74	11.9	16.6	173	0.09	2.82

of hydrothermal activity (Steiner et al., 2001; Orberger et al., 2007; Xu et al., 2013), and some studies specifically point out that the Ni-Mo enriched layers in South China have characteristics of being rich in Ni, Pb, Co, and other elements, indicating that the submarine hydrothermal fluids in the South China sedimentary basin have interacted with basic and ultrabasic rocks and leached metal elements (such as Ni, Pb and Co) from the rocks (Jiang et al., 2006; Zhang et al., 2014; Lan et al., 2017). In contrast, the contemporaneous Cambrian Strata in Tarim did not show similar characteristics, with only slightly Ni enrichment and Co depletion, which indicates totally different chemical composition of the hydrothermal fluid. Meanwhile, the Ni-Mo enriched layers in Tarim are also depleted in Zr and Hf, which exclude the possibility of the hydrothermal fluid interaction with felsic rocks. Previous study has reported underlying rock series containing metamorphic basic-intermediate volcanic rocks in Tarim (Zhu et al., 2018). The hydrothermal system in Tarim probably originated from intermediate magma or migrated upwards through the intermediate rocks in early Cambrian, and leaching amount of Mo, V, U into the seawater.

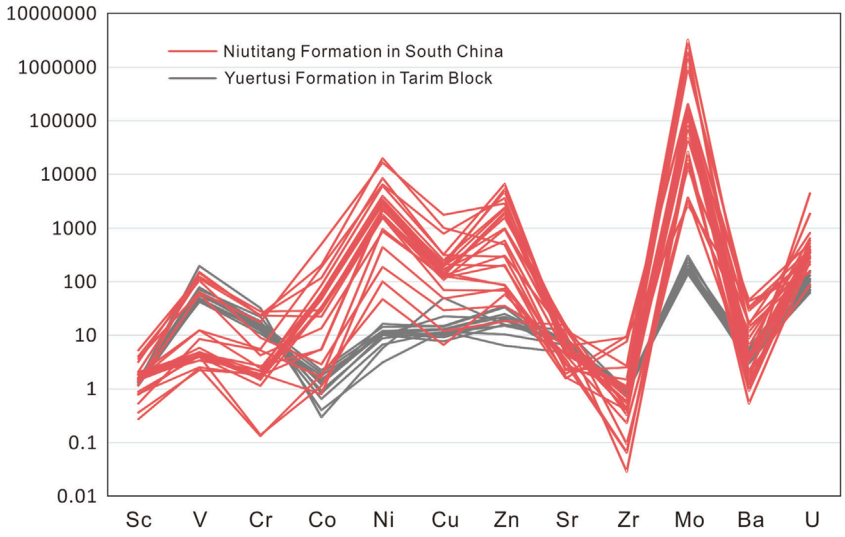

FIGURE 11
Trace element spider diagrams of black shales in the middle section of the Yurtus Formation in the Tarim Basin and Ni-Mo ore layers in the Niutitang Formation in South China. Data of Yurtus Formation in Tarim are from Yu et al. (2009), and data of Niutitang Formation in South China are from Jiang et al. (2006) and Tao et al. (2015).

Taking into account the significant differences in the degree of metal enrichment at the base of the Cambrian strata in the Tarim and South China (differing by 1–3 orders of magnitude), it could be concluded that there are no Ni-Mo enriched layers in Tarim similar to those in South China. Both metal enrichments on the two Blocks were likely influenced by the local hydrothermal activity, only with different types of hydrothermal fluids, which resulted in discrepancy in content and types of their metal elements. Previous studies have suggested that the hydrothermal activity mainly occurred in slope area in South China, which is totally consistent with the distribution of Ni-Mo enriched layers (Zhao et al., 2024). In this study, an active seafloor hydrothermal activity was confirmed in Aksu area. However, given that the limited data published in Tarim, it is difficult to determine the detailed distribution of the hydrothermal system throughout the Tarim basin by now, which await further study. Nevertheless, both continental basins were influenced by hydrothermal activity during the same period, supposedly indicating a period of global submarine hydrothermal activity. The extensive hydrothermal fluids brought abundant metal nutrients and may have been one of the important causes for the increase in marine productivity, biodiversity, and rapid animal evolution (Zhu, 2010). This conclusion needs to be confirmed by further research in the future.

6 Conclusion

Polymetallic Ni-Mo enriched layers have been verified to be widely developed in the black rock series at the base of the Cambrian strata in South China, yet their genesis mechanism remain unsettled. This work has conducted a comprehensive study on the trace and rare earth elements of the black rock series deposited during early Cambrian in Tarim, attempting to make a systematic comparison on metal enrichments between South China and Tarim. The new and previous published data from the Tarim suggest that the black rock series deposited in early Cambrian were mainly enriched in Mo, V, Zn and Cr, with Ni slight enrichment and Co depletion. These metal elements mainly derived from the waning hydrothermal fluids, and precipitated and preserved in sediments in a reduced seawater environment. On the contrary, the contemporaneous black rock series in South China were generally enriched in Mo, V, Zn, Ni and Co, with much higher metal concentrations by 1–3 orders of magnitude. These results could indicate that the polymetallic Ni-Mo enriched layers did not develop in the Tarim and were at least partly derived from the local hydrothermal activities in South China. We further proposed that the early Cambrian may have been an active period of submarine volcanoes, which have provided large number of nutrient elements for the rapid evolution of animals.

Data availability statement

The original contributions presented in the study are included in the article/supplementary material, further inquiries can be directed to the corresponding author.

Author contributions

HW: Conceptualization, Investigation, Methodology, Writing–original draft, Writing–review and editing, Data curation, Formal Analysis. YS: Data curation, Formal Analysis, Investigation, Methodology, Writing–original draft. DW: Conceptualization, Funding acquisition, Project administration, Resources, Validation, Writing–original draft, Writing–review and editing. XS: Formal Analysis, Investigation, Methodology, Writing–review and editing. CC: Formal Analysis, Investigation, Methodology, Writing–review

and editing. PQ: Data curation, Formal Analysis, Investigation, Writing–review and editing.

Funding

The authors declare that financial support was received for the research, authorship, and/or publication of this article. This work was supported by the National Natural Science Foundation of China (42073006) and the National Key Research and Development Program of China (2022YFF0802700).

Acknowledgments

We thank Dr. Ben Yang for his helpful discussions.

Conflict of interest

The authors declare that the research was conducted in the absence of any commercial or financial relationships that could be construed as a potential conflict of interest.

Publisher's note

All claims expressed in this article are solely those of the authors and do not necessarily represent those of their affiliated organizations, or those of the publisher, the editors and the reviewers. Any product that may be evaluated in this article, or claim that may be made by its manufacturer, is not guaranteed or endorsed by the publisher.

References

Algeo, T., and Tribovillard, N. (2009). Environmental analysis of paleoceanographic systems based on molybdenum–uranium covariation. *Chem. Geol.* 268 (3), 211–225. doi:10.1016/j.chemgeo.2009.09.001

Algeo, T. J., and Maynard, J. B. (2008). Trace-metal covariation as a guide to water-mass conditions in ancient anoxic marine environments. *Geosphere* 4 (5), 872–887. doi:10.1130/ges00174.1

Algeo, T. J., Morford, J., and Cruse, A. (2012). *New applications of trace metals as proxies in marine paleoenvironments*. Elsevier, 160–164.

Algeo, T. J., and Rowe, H. (2012). Paleoceanographic applications of trace-metal concentration data. *Chem. Geol.* 324, 6–18. doi:10.1016/j.chemgeo.2011.09.002

Anders, E., and Grevesse, N. (1989). Abundances of the elements: meteoritic and solar. *Geochimica Cosmochimica acta* 53 (1), 197–214. doi:10.1016/0016-7037(89)90286-x

Barrett, T. J., Jarvis, I., and Jarvis, K. E. (1990). Rare earth element geochemistry of massive sulfides-sulfates and gossans on the Southern Explorer Ridge. *Geology* 18 (7), 583–586. doi:10.1130/0091-7613(1990)018<0583:reegom>2.3.co;2

Bau, M. (1996). Controls on the fractionation of isovalent trace elements in magmatic and aqueous systems: evidence from Y/Ho, Zr/Hf, and lanthanide tetrad effect. *Contrib. Mineral. Petr.* 123, 323–333. doi:10.1007/s004100050159

Bau, M., and Koschinsky, A. (2009). Oxidative scavenging of cerium on hydrous Fe oxide: evidence from the distribution of rare earth elements and yttrium between Fe oxides and Mn oxides in hydrogenetic ferromanganese crusts. *Geochem. J.* 43 (1), 37–47. doi:10.2343/geochemj.1.0005

Cawood, P. A., Strachan, R. A., Pisarevsky, S. A., Gladkochub, D. P., and Murphy, J. B. (2016). Linking collisional and accretionary orogens during Rodinia assembly and breakup: implications for models of supercontinent cycles. *Earth Planet. Sci. Lett.* 449, 118–126. doi:10.1016/j.epsl.2016.05.049

Chen, D., Qing, H., Yan, X., and Li, H. (2006). Hydrothermal venting and basin evolution (Devonian, South China): constraints from rare earth element geochemistry of chert. *Sediment. Geol.* 183 (3-4), 203–216. doi:10.1016/j.sedgeo.2005.09.020

Chen, X., Ling, H.-F., Vance, D., Shields-Zhou, G. A., Zhu, M., Poulton, S. W., et al. (2015). Rise to modern levels of ocean oxygenation coincided with the Cambrian radiation of animals. *Nat. Commun.* 6, 7142. doi:10.1038/ncomms8142

Choi, J. H., and Hariya, Y. (1992). Geochemistry and depositional environment of Mn oxide deposits in the Tokoro Belt, northeastern Hokkaido, Japan. *Econ. Geol.* 87 (5), 1265–1274. doi:10.2113/gsecongeo.87.5.1265

Cocherie, A., Calvez, J., and Oudin-Dunlop, E. (1994). Hydrothermal activity as recorded by Red Sea sediments: Sr-Nd isotopes and REE signatures. *Mar. Geol.* 118 (3-4), 291–302. doi:10.1016/0025-3227(94)90089-2

Cook, P. J. (1992). Phosphogenesis around the Proterozoic-Phanerozoic transition. *J. Geol. Soc.* 149 (4), 615–620. doi:10.1144/gsjgs.149.4.0615

Douville, E., Bienvenu, P., Charlou, J. L., Donval, J. P., Fouquet, Y., Appriou, P., et al. (1999). Yttrium and rare earth elements in fluids from various deep-sea hydrothermal systems. *Geochimica Cosmochimica Acta* 63 (5), 627–643. doi:10.1016/s0016-7037(99)00024-1

Gao, P., He, Z., Li, S., Lash, G. G., Li, B., Huang, B., et al. (2018). Volcanic and hydrothermal activities recorded in phosphate nodules from the Lower Cambrian Niutitang Formation black shales in South China. *Palaeogeogr. Palaeoclimatol. Palaeoecol.* 505, 381–397. doi:10.1016/j.palaeo.2018.06.019

Gao, Z., and Fan, T. (2015). Carbonate platform-margin architecture and its influence on Cambrian-Ordovician reef-shoal development, Tarim Basin, NW China. *Mar. Petroleum Geol.* 68, 291–306. doi:10.1016/j.marpetgeo.2015.08.033

Gao, Z., Zhu, X., Wang, D., Pan, C., Yan, B., and Li, J. (2021). Insights into hydrothermal controls and processes leading to the formation of the Late Ediacaran Gaoyan stratiform manganese-carbonate deposit, Southwest China. *Ore Geol. Rev.* 139, 104524. doi:10.1016/j.oregeorev.2021.104524

Guo, Q., Shields, G. A., Liu, C., Strauss, H., Zhu, M., Pi, D., et al. (2007). Trace element chemostratigraphy of two Ediacaran–Cambrian successions in South China: implications for organosedimentary metal enrichment and silicification in the Early Cambrian. *Palaeogeogr. Palaeoclimatol. Palaeoecol.* 254 (1–2), 194–216. doi:10.1016/j.palaeo.2007.03.016

Han, T., Zhu, X., Li, K., Jiang, L., Zhao, C., and Wang, Z. (2015). Metal sources for the polymetallic Ni–Mo–pge mineralization in the black shales of the lower cambrian Niutitang Formation, South China. *Ore Geol. Rev.* 67, 158–169. doi:10.1016/j.oregeorev.2014.11.020

Hatch, J., and Leventhal, J. (1992). Relationship between inferred redox potential of the depositional environment and geochemistry of the upper pennsylvanian (missourian) Stark shale member of the dennis limestone, wabaunsee county, Kansas, USA. *Chem. Geol.* 99 (1-3), 65–82. doi:10.1016/0009-2541(92)90031-y

He, B., Jiao, C., Cai, Z., Liu, R., Meert, J. G., Yun, X., et al. (2021). Soft-sediment deformation structures (SSDS) in the Ediacaran and lower Cambrian succession of the Aksu area, NW Tarim Basin, and their implications. *Palaeogeogr. Palaeoclimatol. Palaeoecol.* 567, 110237. doi:10.1016/j.palaeo.2021.110237

He, T., Lu, S., Li, W., Sun, D., Pan, W., Zhang, B., et al. (2020). Paleoweathering, hydrothermal activity and organic matter enrichment during the formation of earliest Cambrian black strata in the northwest Tarim Basin, China. *J. Petroleum Sci. Eng.* 189, 106987. doi:10.1016/j.petrol.2020.106987

Jiang, S.-Y., Chen, Y.-Q., Ling, H.-F., Yang, J.-H., Feng, H.-Z., and Ni, P. (2006). Trace-and rare-earth element geochemistry and Pb–Pb dating of black shales and intercalated Ni–Mo–PGE–Au sulfide ores in Lower Cambrian strata, Yangtze Platform, South China. *Miner. Deposita* 41 (5), 453–467. doi:10.1007/s00126-006-0066-6

Jiang, S.-Y., Yang, J.-H., Ling, H.-F., Chen, Y.-Q., Feng, H.-Z., Zhao, K.-D., et al. (2007). Extreme enrichment of polymetallic Ni–Mo–PGE–Au in Lower Cambrian black shales of South China: an Os isotope and PGE geochemical investigation. *Palaeogeogr. Palaeoclimatol. Palaeoecol.* 254 (1-2), 217–228. doi:10.1016/j.palaeo.2007.03.024

Johannesson, K. H., Hawkins Jr, D. L., and Cortés, A. (2006). Do Archean chemical sediments record ancient seawater rare earth element patterns? *Geochimica Cosmochimica Acta* 70 (4), 871–890. doi:10.1016/j.gca.2005.10.013

Jones, B., and Manning, D. A. (1994). Comparison of geochemical indices used for the interpretation of palaeoredox conditions in ancient mudstones. *Chem. Geol.* 111 (1-4), 111–129. doi:10.1016/0009-2541(94)90085-x

Knoll, A. H., and Carroll, S. B. (1999). Early animal evolution: emerging views from comparative biology and geology. *science* 284 (5423), 2129–2137. doi:10.1126/science.284.5423.2129

Lan, Z., Li, X.-H., Chu, X., Tang, G., Yang, S., Yang, H., et al. (2017). SIMS U-Pb zircon ages and Ni-Mo-PGE geochemistry of the lower Cambrian Niutitang Formation in South China: constraints on Ni-Mo-PGE mineralization and stratigraphic correlations. *J. Asian Earth Sci.* 137, 141–162. doi:10.1016/j.jseaes.2016.12.046

Lawrence, M. G., and Kamber, B. S. (2006). The behaviour of the rare earth elements during estuarine mixing—revisited. *Ma. Chem.* 100, 147–161. doi:10.1016/j.marchem.2005.11.007

Lehmann, B., Frei, R., Xu, L., and Mao, J. (2016). Early Cambrian black shale-hosted Mo-Ni and V mineralization on the rifted margin of the Yangtze Platform, China: reconnaissance chromium isotope data and a refined metallogenic model. *Econ. Geol.* 111 (1), 89–103. doi:10.2113/econgeo.111.1.89

Lehmann, B., Nagler, T. F., Holland, H. D., Wille, M., Mao, J., Pan, J., et al. (2007). Highly metalliferous carbonaceous shale and Early Cambrian seawater. *Geology* 35 (5), 403–406. doi:10.1130/g23543a.1

Li, F., Lü, X., Chen, J., Wang, R., Wang, Y., and Chen, Z. (2022). Palaeo-environmental evolution and organic matter enrichment of Eopalaeozoic shales, northwestern Tarim Basin, China: integrated organic and inorganic geochemistry approach. *Palaeogeogr. Palaeoclimatol. Palaeoecol.* 601, 111123. doi:10.1016/j.palaeo.2022.111123

Li, G. (2013). *How to define the lower boundary of the Cambrian Stage 2: a biostratigraphic marker or a geochemical one? Lund*. Sweden, 179. 9–19 June 2013.

Li, S., Zhao, S., Liu, X., Cao, H., Yu, S., Li, X., et al. (2018). Closure of the proto-tethys ocean and early paleozoic amalgamation of microcontinental blocks in east asia. *Earth-Science Rev.* 186, 37–75. doi:10.1016/j.earscirev.2017.01.011

Ling, H.-F., Chen, X., Li, D., Wang, D., Shields-Zhou, G. A., and Zhu, M. (2013). Cerium anomaly variations in Ediacaran–earliest Cambrian carbonates from the Yangtze Gorges area, South China: implications for oxygenation of coeval shallow seawater. *Precambrian Res.* 225, 110–127. doi:10.1016/j.precamres.2011.10.011

Litvinova, T. V. (2007). Composition, morphology, and origin of phosphate pellets: evidence from phosphorites of the Lesser Karatau. *Lithology Mineral Resour.* 42, 384–399. doi:10.1134/s0024490207040050

Liyuan, W., Qingjun, G., Changqiu, Z., Rongfei, W., Yinan, D., Xiaokun, H., et al. (2021). Trace and rare earth elements geochemistry of sedimentary rocks in the Ediacaran-Cambrian transition from the Tarim Basin, Northwest China: constraints for redox environments. *Precambrian Res.* 352, 105942. doi:10.1016/j.precamres.2020.105942

Long, J., and Luo, K. (2017). Trace element distribution and enrichment patterns of Ediacaran-early Cambrian, Ziyang selenosis area, Central China: constraints for the origin of Selenium. *J. Geochem. Explor.* 172, 211–230. doi:10.1016/j.gexplo.2016.11.010

Lv, D., Song, Y., Shi, L., Wang, Z., Cong, P., and van Loon, A. T. (2020). The complex transgression and regression history of the northern margin of the Palaeogene Tarim Sea (NW China), and implications for potential hydrocarbon occurrences. *Mar. petroleum Geol.* 112, 104041. doi:10.1016/j.marpetgeo.2019.104041

Lyons, T. W., Reinhard, C. T., and Planavsky, N. J. (2014). The rise of oxygen in Earth's early ocean and atmosphere. *Nature* 506 (7488), 307–315. doi:10.1038/nature13068

Mao, J., Lehmann, B., Du, A., Zhang, G., Ma, D., Wang, Y., et al. (2002). Re-Os dating of polymetallic Ni-Mo-PGE-Au mineralization in Lower Cambrian black shales of South China and its geologic significance. *Econ. Geol.* 97 (5), 1051–1061. doi:10.2113/97.5.1051

Martínez-Ruiz, F., Ortega-Huertas, M., and Palomo, I. (1999). Positive Eu anomaly development during diagenesis of the K/T boundary ejecta layer in the Agost section (SE Spain): implications for trace-element remobilization. *Terra nova.* 11 (6), 290–296. doi:10.1046/j.1365-3121.1999.00261.x

Mazumdar, A., Banerjee, D., Schidlowski, M., and Balaram, V. (1999). Rare-earth elements and stable isotope geochemistry of early cambrian chert-phosphorite assemblages from the lower tal Formation of the krol belt (lesser himalaya, India). *Chem. Geol.* 156 (1-4), 275–297. doi:10.1016/s0009-2541(98)00187-9

Michard, A., and Albarède, F. (1986). The REE content of some hydrothermal fluids. *Chem. Geol.* 55 (1-2), 51–60. doi:10.1016/0009-2541(86)90127-0

Mills, R. A., and Elderfield, H. (1995). Rare earth element geochemistry of hydrothermal deposits from the active TAG Mound, 26°N Mid-Atlantic Ridge. *Geochimica cosmochimica acta* 59 (17), 3511–3524. doi:10.1016/0016-7037(95)00224-n

Murray, R. W., Ten Brink, M. R. B., Gerlach, D. C., Russ III, G. P., and Jones, D. L. (1991). Rare earth, major, and trace elements in chert from the Franciscan Complex and Monterey Group, California: assessing REE sources to fine-grained marine sediments. *Geochimica Cosmochimica Acta* 55 (7), 1875–1895. doi:10.1016/0016-7037(91)90030-9

Nozaki, Y., Zhang, J., and Amakawa, H. (1997). The fractionation between Y and Ho in the marine environment. *Earth Planet. Sci. Lett.* 148 (1-2), 329–340. doi:10.1016/s0012-821x(97)00034-4

Och, L. M., and Shields-Zhou, G. A. (2012). The Neoproterozoic oxygenation event: environmental perturbations and biogeochemical cycling. *Earth-Science Rev.* 110 (1–4), 26–57. doi:10.1016/j.earscirev.2011.09.004

Olivarez, A. M., and Owen, R. M. (1991). The europium anomaly of seawater: implications for fluvial versus hydrothermal REE inputs to the oceans. *Chem. Geol.* 92 (4), 317–328. doi:10.1016/0009-2541(91)90076-4

Orberger, B., Vymazalova, A., Wagner, C., Fialin, M., Gallien, J. P., Wirth, R., et al. (2007). Biogenic origin of intergrown Mo-sulphide- and carbonaceous matter in Lower Cambrian black shales (Zunyi Formation, southern China). *Chem. Geol.* 238 (3–4), 213–231. doi:10.1016/j.chemgeo.2006.11.010

Owen, A., Armstrong, H., and Floyd, J. (1999). Rare earth element geochemistry of upper Ordovician cherts from the Southern Uplands of Scotland. *J. Geol. Soc.* 156 (1), 191–204. doi:10.1144/gsjgs.156.1.0191

Pi, D.-H., Liu, C.-Q., Shields-Zhou, G. A., and Jiang, S.-Y. (2013). Trace and rare earth element geochemistry of black shale and kerogen in the early Cambrian Niutitang Formation in Guizhou province, South China: constraints for redox environments and origin of metal enrichments. *Precambrian Res.* 225, 218–229. doi:10.1016/j.precamres.2011.07.004

Qian, Y., Feng, W., Li, G., Yang, A., Feng, M., Zhao, X., et al. (2009). Taxonomy and biostratigraphy of the early Cambrian univalved mollusc fossils from Xinjiang. *Acta Micropalaeontologica Sin.* 26 (3), 193–210. (in Chinese with English abstract).

Ramseyer, K., Amthor, J. E., Matter, A., Pettke, T., Wille, M., and Fallick, A. E. (2013). Primary silica precipitate at the precambrian/cambrian boundary in the SouthSouth Oman salt basin, sultanate of Oman. *Mar. Petroleum Geol.* 39 (1), 187–197. doi:10.1016/j.marpetgeo.2012.08.006

Reinhard, C. T., Planavsky, N. J., Gill, B. C., Ozaki, K., Robbins, L. J., Lyons, T. W., et al. (2017). Evolution of the global phosphorus cycle. *Nature* 541 (7637), 386–389. doi:10.1038/nature20772

Sakai, H. (1968). Isotopic properties of sulfur compounds in hydrothermal processes. *Geochem. J.* 2 (1), 29–49. doi:10.2343/geochemj.2.29

Shields, G., and Stille, P. (2001). Diagenetic constraints on the use of cerium anomalies as palaeoseawater redox proxies: an isotopic and REE study of Cambrian phosphorites. *Chem. Geol.* 175 (1-2), 29–48. doi:10.1016/s0009-2541(00)00362-4

Shields-Zhou, G., and Och, L. (2011). The case for a Neoproterozoic oxygenation event: geochemical evidence and biological consequences. *GSa Today* 21 (3), 4–11. doi:10.1130/gsatg102a.1

Shu, D., Isozaki, Y., Zhang, X., Han, J., and Maruyama, S. (2014). Birth and early evolution of metazoans. *Gondwana Res.* 25 (3), 884–895. doi:10.1016/j.gr.2013.09.001

Sláma, J., Košler, J., Condon, D. J., Crowley, J. L., Gerdes, A., Hanchar, J. M., et al. (2008). Plešovice zircon—a new natural reference material for U–Pb and Hf isotopic microanalysis. *Chem. Geol.* 249 (1), 1–35. doi:10.1016/j.chemgeo.2007.11.005

Steiner, M., Li, G., Yi, Q., Zhu, M., and Erdtmann, B. D. (2007). Neoproterozoic to Early Cambrian small shelly fossil assemblages and a revised biostratigraphic correlation of the Yangtze Platform (China). *Palaeogeogr. Palaeoclimatol. Palaeoecol.* 254 (1-2), 67–99. doi:10.1016/j.palaeo.2007.03.046

Steiner, M., Wallis, E., Erdtmann, B. D., Zhao, Y. L., and Yang, R. D. (2001). Submarine-hydrothermal exhalative ore layers in black shales from South China and associated fossils - insights into a Lower Cambrian facies and bio-evolution. *Palaeogeogr. Palaeoclimatol. Palaeoecol.* 169 (3-4), 165–191. doi:10.1016/s0031-0182(01)00208-5

Steiner, M., Zhu, M., Zhao, Y., and Erdtmann, B.-D. (2005). Lower Cambrian burgess shale-type fossil associations of south China. *Palaeogeogr. Palaeoclimatol. Palaeoecol.* 220 (1), 129–152. doi:10.1016/j.palaeo.2003.06.001

Tanaka, K., Tani, Y., Takahashi, Y., Tanimizu, M., Suzuki, Y., Kozai, N., et al. (2010). A specific Ce oxidation process during sorption of rare earth elements on biogenic Mn oxide produced by Acremonium sp. strain KR21-2. *Geochimica Cosmochimica Acta* 74 (19), 5463–5477. doi:10.1016/j.gca.2010.07.010

Tao, H., Zhu, X., Li, K., Lei, J., Zhao, C., and Wang, Z. (2015). Metal sources for the polymetallic Ni–Mo–pge mineralization in the black shales of the lower cambrian Niutitang Formation, South China. *Ore Geol. Rev.* 67, 158–169. doi:10.1016/j.oregeorev.2014.11.020

Taylor, S. R., and McLennan, S. M. (1985). *The continental crust: its composition and evolution*.

Tribovillard, N., Algeo, T. J., Baudin, F., and Riboulleau, A. (2012). Analysis of marine environmental conditions based onmolybdenum–uranium covariation—applications to Mesozoic paleoceanography. *Chem. Geol.* 324–325 (0), 46–58. doi:10.1016/j.chemgeo.2011.09.009

Tribovillard, N., Algeo, T. J., Lyons, T., and Riboulleau, A. (2006). Trace metals as paleoredox and paleoproductivity proxies: an update. *Chem. Geol.* 232 (1-2), 12–32. doi:10.1016/j.chemgeo.2006.02.012

Wang, H., Wang, D., Wei, G.-Y., Ling, H.-F., Struck, U., Wei, W., et al. (2022a). Increases in marine environmental heterogeneity during the early animal innovations: evidence from nitrogen isotopes in South China. *Precambrian Res.* 369, 106501. doi:10.1016/j.precamres.2021.106501

Wang, Y., Chen, J., Shen, W., and Li, M. (2022b). Mechanism of organic matter accumulation in black shales of the yuertusi Formation in the Tarim Basin: insights from paleoenvironmental variation during the early cambrian. *Front. Earth Sci.* 10, 879658. doi:10.3389/feart.2022.879658

Wei, G.-Y., Planavsky, N. J., He, T., Zhang, F., Stockey, R., Cole, D. B., et al. (2021). Global marine redox evolution from the late Neoproterozoic to the early Paleozoic constrained by the integration of Mo and U isotope records. *Earth-Science Rev.* 214, 103506. doi:10.1016/j.earscirev.2021.103506

Xiao, B. (1989). Review of the age of uyirtus Formation in the light of the discovery of Anabarites. *Xinjiang Geol.* 4, 35–39. (in Chinese with English abstract).

Xu, L., Lehmann, B., and Mao, J. (2013). Seawater contribution to polymetallic Ni–Mo–PGE–Au mineralization in Early Cambrian black shales of South China: evidence from Mo isotope, PGE, trace element, and REE geochemistry. *Ore Geol. Rev.* 52, 66–84. doi:10.1016/j.oregeorev.2012.06.003

Xu, L., Lehmann, B., Mao, J., Nägler, T. F., Neubert, N., Böttcher, M. E., et al. (2012). Mo isotope and trace element patterns of Lower Cambrian black shales in South China: multi-proxy constraints on the paleoenvironment. *Chem. Geol.* 318, 45–59. doi:10.1016/j.chemgeo.2012.05.016

Xu, L. G., Lehmann, B., Mao, J. W., Qu, W. J., and Du, A. D. (2011). Re-Os age of polymetallic Ni-Mo-pge-Au mineralization in early cambrian black shales of SouthSouth China-A reassessment. *Econ. Geol.* 106 (3), 511–522. doi:10.2113/econgeo.106.3.511

Yang, Z., Wu, P., Fu, Y., Qiao, W., Qin, Y., Li, C., et al. (2022). Coupling of the redox history and enrichment of Ni-Mo in black shale during the early Cambrian: constraints from S-Fe isotopes and trace elements of pyrite, South China. *Ore Geol. Rev.* 143, 104749. doi:10.1016/j.oregeorev.2022.104749

Yao, C., Ma, D., Ding, H., Zhang, X., and Huang, H. (2014). Trace elements and stable isotopic geochemistry of an Early Cambrian chert-phosphorite unit from the lower Yurtus Formation of the Sugetbrak section in the Tarim Basin. *Sci. China Earth Sci.* 57, 454–464. doi:10.1007/s11430-013-4760-9

Yao, J., Xiao, S., Yin, L., Li, G., and Yuan, X. (2005). Basal Cambrian microfossils from the Yurtus and Xishanblaq formations (Tarim, north-west China): systematic revision and biostratigraphic correlation of Micrhystridium-like acritarchs. *Palaeontology* 48 (4), 687–708. doi:10.1111/j.1475-4983.2005.00484.x

Yu, B., Dong, H., Widom, E., Chen, J., and Lin, C. (2009). Geochemistry of basal Cambrian black shales and cherts from the Northern Tarim Basin, Northwest China: implications for depositional setting and tectonic history. *J. Asian Earth Sci.* 34 (3), 418–436. doi:10.1016/j.jseaes.2008.07.003

Yue, Z. (1992). A new species of early Cambrian Lapworthella from Xinjiang, China with discussions on some problems concerning this genus. *Acta Palaeontol. Sin.* 31 (1), 108–117. doi:10.19800/j.cnki.aps.1992.01.009 (in Chinese with English abastract).

Yue, Z., and Gao, L. (1992). Paleontology, biostratigraphy and geological significance of the Early Cambrian protoconodonts and other skeletal microfossils from Aksu-Wushi region, Xinjiang, China. *Bull. Inst. Geol. Chin. Acad. Geol. Sci.* 23, 133–160. (in Chinese with English abstract).

Zeng, H., Xu, Z., Liu, W., Janson, X., and Fu, Q. (2022). Seismic-informed carbonate shelf-to-basin transition in deeply buried Cambrian strata, Tarim Basin, China. *Mar. Petroleum Geol.* 136, 105448. doi:10.1016/j.marpetgeo.2021.105448

Zhang, C., Guan, S., Wu, L., Ren, R., Wang, L., and Wu, X. (2020). Depositional environments of early Cambrian marine shale, northwestern Tarim Basin, China: implications for organic matter accumulation. *J. Petroleum Sci. Eng.* 194, 107497. doi:10.1016/j.petrol.2020.107497

Zhang, C. L., Li, H. K., Santosh, M., Li, Z. X., Zou, H. B., Wang, H., et al. (2012). Precambrian evolution and cratonization of the Tarim Block, NW China: petrology, geochemistry, Nd-isotopes and U–Pb zircon geochronology from Archaean gabbro-TTG–potassic granite suite and Paleoproterozoic metamorphic belt. *J. Asian Earth Sci.* 47, 5–20. doi:10.1016/j.jseaes.2011.05.018

Zhang, J., Amakawa, H., and Nozaki, Y. (1994). The comparative behaviors of yttrium and lanthanides in the seawater of the North Pacific. *Geophys. Res. Lett.* 21 (24), 2677–2680. doi:10.1029/94gl02404

Zhang, K., Zhu, X., Wood, R. A., Shi, Y., Gao, Z., and Poulton, S. W. (2018). Oxygenation of the Mesoproterozoic ocean and the evolution of complex eukaryotes. *Nat. Geosci.* 11 (5), 345–350. doi:10.1038/s41561-018-0111-y

Zhang, X., Shu, D., Han, J., Zhang, Z., Liu, J., and Fu, D. (2014). Triggers for the Cambrian explosion: hypotheses and problems. *Gondwana Res.* 25 (3), 896–909. doi:10.1016/j.gr.2013.06.001

Zhang, Y., Wang, Z., Yang, X., Huang, L., Li, Y., and Qin, L. (2022). Petrological and Ni-Mo isotopic evidence for the genesis of the Ni-and Mo-sulfide extremely enriched early Cambrian black shale from Southwest China. *Chem. Geol.* 598, 120812. doi:10.1016/j.chemgeo.2022.120812

Zhang, Z., Zhu, W., Shu, L., Su, J., and Zheng, B. (2009). Neoproterozoic ages of the Kuluketage diabase dyke swarm in Tarim, NW China, and its relationship to the breakup of Rodinia. *Geol. Mag.* 146 (1), 150–154. doi:10.1017/s0016756808005839

Zhang, Z.-l., Ou, Z.-j., Li, H.-l., Li, S.-j., Wu, J., and Meng, F.-w. (2023). Early Cambrian microfossils from the cherts in carbonates of the Kuruktag area, the Tarim block. *Carbonates Evaporites* 38 (2), 32. doi:10.1007/s13146-023-00854-0

Zhao, B., Long, X., and Chang, C. (2024). Early Cambrian sedimentary rocks in South China: a link between oceanic oxygenation and biological explosion. *Earth-Science Rev.* 250, 104708. doi:10.1016/j.earscirev.2024.104708

Zhou, X., Chen, D., Dong, S., Zhang, Y., Guo, Z., Wei, H., et al. (2015). Diagenetic barite deposits in the Yurtus Formation in Tarim Basin, NW China: implications for barium and sulfur cycling in the earliest cambrian. *Precambrian Res.* 263, 79–87. doi:10.1016/j.precamres.2015.03.006

Zhou, X., Chen, D., Qing, H., Qian, Y., and Wang, D. (2014). Submarine silica-rich hydrothermal activity during the earliest cambrian in the Tarim Basin, northwest China. *Int. Geol. Rev.* 56 (15), 1906–1918. doi:10.1080/00206814.2014.968885

Zhu, B., Yang, T., Wang, J., Chen, X., Pan, W., and Chen, Y. (2022). Multiple controls on the paleoenvironment of the early Cambrian black shale-chert in the northwest Tarim Basin, NW China: trace element, iron speciation and Mo isotopic evidence. *Mar. Petroleum Geol.* 136, 105434. doi:10.1016/j.marpetgeo.2021.105434

Zhu, G., Du, D., Chen, W., Sun, Q., Li, T., Zhang, Z., et al. (2018). Discovery of Precambrian thick black mudstones and its implication for hydrocarbon exploration in the southwest Tarim Basin. *Petroleum Res.* 3 (2), 124–131. doi:10.1016/j.ptlrs.2018.06.006

Zhu, M. (2010). The origin and Cambrian explosion of animals: fossil evidences from China. *Acta Palaeontol. Sin.* 49 (03), 269–287. doi:10.19800/j.cnki.aps.2010.03.001 (In Chinese with English abstract).

Zhu, M., Zhang, J., Yang, A., Li, G., Steiner, M., and Erdtmann, B. D. (2003). Sinian-Cambrian stratigraphic framework for shallow-to deep-water environments of the Yangtze Platform: an integrated approach. *Prog. Nat. Sci.* 13 (12), 951–960. doi:10.1080/10020070312331344710